

Algorithms for Reconstructing B Cell Lineages in the Presence of Context-Dependent Somatic Hypermutation

Yongkang Li¹[0000-0003-1785-4689], Kevin Wiehe¹, and Scott C. Schmidler¹[0009-0006-3733-3716]

Duke University, Durham NC 27708, USA

Abstract. We introduce a method for approximating posterior probabilities of phylogenetic trees and reconstructing ancestral sequences under models of sequence evolution with site-dependence, where standard phylogenetic likelihood computations (pruning) fail. Our approach uses a combined data-augmentation and importance sampling scheme. A key advantage of our approach is the ability to leverage existing highly optimized phylogenetic software. We apply our approach to the reconstruction of B cell receptor affinity maturation lineages from high-throughput repertoire sequencing data and evaluate the impact of incorporating site-dependence on the reconstruction accuracy of both trees and ancestral sequences. We show that accounting for context-dependence during inference always improves the estimates of both ancestral sequences and lineage trees on simulated datasets. We also examine the impact of incorporating priors based on VDJ recombination models, and find that they significantly improve ancestral sequence reconstruction in germline-encoded regions, but increase errors in non-templated nucleotides. We propose a modified, piecewise prior to address this and demonstrate that it improves empirical reconstruction accuracy. We apply our approach to the analysis of the HIV broadly neutralizing antibodies DH270 and CH235 which are important targets of current vaccine design efforts. **Code availability:** <https://github.com/YongkangLi/PhyConD>

Keywords: Affinity Maturation · Computational Immunology · Phylogenetic Tree · Context Dependence · Sequential Monte Carlo.

1 Introduction

To prevent infectious diseases, the immune system must recognize and clear foreign pathogens capable of host infection. The adaptive immune system does so using B cells with receptors specifically tailored to bind pathogens. Facing a near-infinite variety of pathogen protein surfaces, B cells rely on two diversification methods: 1) initial gene segment shuffling (VDJ recombination) to enable weak binding to the diversity of antigens encountered, and 2) a refinement step (affinity maturation) that substantially improves binding and BCR-antigen recognition specificity, accomplished via somatic hypermutation (SHM). Understanding of this process and design of new vaccines is greatly aided by computational and statistical analysis of data from high-throughput B cell repertoire sequencing. A key challenge is accurate inference of BCR lineages and unmutated common ancestors, and significant progress has been made on these tools [23, 35, 27, 6]. However, existing methods rely on conventional “independent-site” mutation models from molecular phylogenetics and unlike mutational processes elsewhere in the genome, these models do not adequately capture the SHM process, which is mediated by the enzyme activation induced cytidine deaminase (AID). Critically, AID activity is *sequence-context dependent*, targeting sites in certain favored motifs. Unfortunately, incorporation of context-dependent mutation models makes standard phylogenetic calculations intractable. Here we develop algorithms for reconstructing B cell lineages under context-dependent SHM models. We build on recent work on approximating pairwise sequence evolution probabilities [31, 28, 29], extending these in non-trivial ways to trees using Monte Carlo methods of data augmentation, importance sampling, and sequential Monte Carlo. Notably, our approach can be implemented directly using existing phylogenetics software.

2 Background

2.1 BnAbs, Sequential Vaccine Design, and B Cell Lineages

The goal of vaccination is to induce antibodies – secreted versions of B cell receptors (BCRs) – that neutralize pathogens and protect against infection. In infection, successive rounds of mutation and selection for antigen affinity (*affinity maturation*) enables B cells to recognize pathogens with specificity. However, rapidly mutating viruses (HIV, influenza, SARS-CoV-2) escape this B cell response by viral diversification. It is thus desired to elicit *broadly neutralizing* antibodies (bnAbs), but these are rarely elicited due to a variety of factors [47]: low precursor frequencies in the human B cell receptor repertoire [12, 20], highly mutated, and containing essential mutations that are highly improbable, creating acquisition bottlenecks [49, 38, 31]. Traditional vaccine design strategies have proven ineffective at eliciting bnAbs, motivating new strategies using known bnAbs as templates to design immunogens to guide B cell maturation the bnAb [11, 21, 12, 41, 24]. *Sequential prime-boosting* aims to first induce low-frequency bnAb precursors with a *priming* immunogen, then mature them with additional *boosting* immunogens, and relies heavily on inferring the precursor BCR sequence (the unmutated common ancestor (UCA)) from observed, clonally-related sequences [23, 11]. More generally reconstruction of B cell *lineage* - the set of affinity maturation pathways for clone members - provides insight into maturation bottlenecks and also precursors to serve as intermediate vaccine targets. Existing lineage reconstruction methods such as Cloanalyst [23], IgOR [27], Partis [35] and LinearHam [6] combine phylogenetic inference with models of VDJ recombination, but follow the vast majority of molecular phylogenetics in assuming that sequence positions evolve independently; this assumption is critical to tractability of phylogenetic inference. While appealing in their simplicity and computational convenience, these independent-site models fail to capture the critical context-dependence of SHM in affinity maturation.

2.2 Affinity Maturation of B Cell Receptors: Context-Dependent Somatic Hypermutation

Unlike genomic mutation, SHM is mediated by a single enzyme AID, which induces mismatch lesions in DNA - and subsequent error-prone repair - that leads to point mutations in BCRs [45]. Critically AID activity is *sequence dependent*, targeting certain favored motifs (“hot spots”) and disfavoring others (“cold spots”).

S5F model and ARMADiLLO: We previously developed ARMADiLLO [49] for simulating SHM using context-dependent mutation probabilities from the S5F model [54], which captures context-dependence of SHM using context-dependent site-mutation and substitution probabilities derived from NGS data [54] for the central nucleotide of 1,024 5-mer motifs, given its (2 upstream and 2 downstream) neighboring bases. The

model parameterizes mutation probabilities as a product of mutability scores and substitution probabilities. ARMADiLLO has been used to forward-simulate SMH and as a null model to test for selection [49, 44]. Unfortunately, this more realistic SHM model cannot be used in existing lineage reconstruction algorithms [23, 27, 35, 6], as context-dependent mutation models directly violate the independent-site assumption that makes standard phylogenetic calculations (pruning) tractable. Since we might expect improved SHM models to provide improved reconstruction of UCAs and lineages, it is of great interest to develop methods for B cell lineage reconstruction which can handle context-dependent mutation models such as S5F/ARMADiLLO.

3 Background

3.1 Standard Models of DNA Evolution

Let $\mathbf{x} = (x_1, \dots, x_\ell)$ and $\mathbf{y} = (y_1, \dots, y_\ell)$ denote two nucleotide sequences of length ℓ , where $x_i, y_i \in \mathcal{A}$ for $\mathcal{A} = \{\text{A,C,G,T}\}$. Standard phylogenetic models assume that each x_i evolves independently according to a time-homogeneous continuous-time Markov chain (CTMC) defined by rate matrices $\mathbf{Q}^{(i)}$ with rates $\mathbf{Q}_{ab}^{(i)} = \gamma^{(i)}(b; a)$ where $\gamma^{(i)} : \mathcal{A}^2 \rightarrow (0, +\infty)$ specifies the rate at which site i mutates from a to b . The *independent-site* assumption allows the straightforward calculation of sequence transition probabilities by

$$p_{(T, \mathbf{Q})}(\mathbf{y} \mid \mathbf{x}) := \Pr(\mathbf{x}(t) = \mathbf{y} \mid \mathbf{x}(0) = \mathbf{x}) = \prod_{i=1}^{\ell} p(y_i \mid x_i, t) = \prod_{i=1}^{\ell} (e^{tQ^{(i)}})_{x_i y_i} \quad (1)$$

where $\mathbf{x}(t) = (x_1(t), \dots, x_n(t))$ denotes the state of the sequence at time t .

3.2 Context-Dependent Mutation Models

The independent site assumption, while computationally convenient, fails to capture a variety of known effects which induce dependence between sites; examples include include CpG di-nucleotide mutability [33], structural constraints in RNA and proteins [36], and enzyme-driven somatic hypermutation in B-cell affinity maturation [49, 31]. A variety of models have been introduced to account for these various effects, most of which can be written as *context-dependent* rate matrices [30]. For nucleotide sequence $\mathbf{x} = (x_1, x_2, \dots, x_\ell)$, let $\tilde{x}_i = (x_{i-k}, \dots, x_i, \dots, x_{i+k})$ denote the *context* of site x_i for $i \in \{1, \dots, \ell\}$. Relaxing the independent-site assumption, we can define a *dependent site model* (DSM) with sites evolving under a time-*inhomogeneous* CTMC and the rate at which x_i mutates to $b \in \mathcal{A}$ in context \tilde{x}_i given by

$$\tilde{\gamma}^{(i)}(b; \tilde{x}_i) := \phi(b; \tilde{x}_i) \gamma^{(i)}(b; x_i) \quad (2)$$

for γ_i the context-independent rate and $\phi : \mathcal{A}^{2k+1} \rightarrow (0, +\infty)$ a context-dependent multiplier; then site i exits x_i at rate $\tilde{\gamma}^{(i)}(\cdot; \tilde{x}_i) := \sum_{b \in \mathcal{A} \setminus \{x_i\}} \tilde{\gamma}^{(i)}(b; \tilde{x}_i)$ and sequence \mathbf{x} mutates at total rate $\tilde{\gamma}(\cdot; \mathbf{x}) := \sum_{i=1}^{\ell} \tilde{\gamma}^{(i)}(\cdot; \tilde{x}_i)$. Under DSMs, the calculation of sequence transition probabilities takes the form

$$p_{(T, \tilde{\mathbf{Q}})}(\mathbf{y} \mid \mathbf{x}) = (e^{t\tilde{\mathbf{Q}}})_{\mathbf{xy}} \quad (3)$$

for $\tilde{\mathbf{Q}}$ the $a^\ell \times a^\ell$ rate matrix of the CTMC on the space of all sequences defined by $\tilde{\mathbf{Q}}_{\mathbf{xx}'} = \tilde{\gamma}^{(i)}(b; \tilde{x}_i)$ if $d_H(\mathbf{x}, \mathbf{x}') = 1$ and $x_i \neq x'_i = b$, and 0 if $d_H(\mathbf{x}, \mathbf{x}') > 1$. For notational simplicity, all models are assumed to be position-independent, eliminating the site-superscript on rates and rate matrices. Figure 1a illustrates how, even when contexts are local, dependence propagates through time to link all sites along the sequence. ARMADiLLO uses a 2-nearest-neighbor 5mer context, with each site i assigned mutability score $m(\cdot; \tilde{x}_i)$ and substitution probability matrix $\eta(x'_i; \tilde{x}_i)$, to form context-dependent rates (2). Mutability scores and substitution probabilities come from S5F [54] based on synonomous mutations in published NGS data.

3.3 Models of BCR Diversification for Lineage Reconstruction

As noted VDJ recombination plays a critical role in diversification, generating the initial gene segment rearrangement upon which SMH operates [19, 46]. Probabilistic hidden Markov models (HMMs) have been successfully applied to model VDJ recombination for clonal UCA reconstruction [23, 6]. These methods marry an independent-site mutation model (1) for SHM with an HMM for stochastic VDJ shuffling. In Section 4.6 below, we consider the incorporation of existing VDJ-models as prior distributions on the UCA, with a likelihood calculated from our dependent-site SHM model, using the methods described in the next section.

4 Methods

We introduce two algorithms for phylogenetic inference under context-dependent models of SMH. We first consider inference based only on the observed clonal sequences (no VDJ recombination model); we refer to this as the *pure phylogenetic model*. Incorporation of VDJ models is considered in Section 4.6.

4.1 Bayesian Lineage Reconstruction: the Pure Phylogenetic Model

The posterior distribution under the pure phylogenetic model is $\pi_{PP}(g, \Psi | Y) \propto p(Y | g, \Psi) f_G(g) f_P(\Psi)$, where Ψ denotes parameters of the evolutionary model (rate matrices), g the genealogy (tree topology & branch lengths), and $Y = \{Y^1, \dots, Y^k\}$ the set of observed sequences $Y^i = (Y_1^i, \dots, Y_\ell^i)$. (For notational simplicity we assume sequences are equal length ℓ , i.e. Y is a multiple alignment). Here f_P and f_G are prior distributions and $p(Y | g, \Psi)$ the marginal likelihood of the observed sequences for a given tree g , the form of which differs between the ISM and DSM, with parameters denoted Ψ_0 and Ψ_1 respectively.

4.2 Marginal likelihood calculation

Evaluating $p(Y | g, \Psi)$ requires marginalizing over unobserved evolutionary histories of Y . For $\mathcal{P}^{(T)} : [0, T] \rightarrow \mathcal{A}^\ell$ an evolutionary path over time $[0, T]$ and $\mathcal{P}^{(T)}$ the set of such paths, (3) can be written [32, 37, 30]:

$$p_{(T, \tilde{\mathbf{Q}})}(\mathbf{y} | \mathbf{x}) = \int_{\mathcal{P}^{(T)}} p_{(T, \tilde{\mathbf{Q}})}(\mathbf{y}, \mathcal{P}^{(T)} | \mathbf{x}) \nu(d\mathcal{P}). \quad (4)$$

Extending this to trees let $\mathcal{P}^{(g)} = (\mathcal{P}^{(t_e)})_{e \in E(g)}$ be a *tree-path*, for edge set $E(g)$ of g and branch length t_e , and edge paths constrained to share internal node sequences. and let $\mathcal{P}^{(g)}$ be the set of tree-paths. Then

$$p(Y | g, \Psi) = \sum_{\mathbf{x}} p(Y, \mathbf{x} | g, \Psi) = \sum_{\mathbf{x}} \int_{\mathcal{P}^{(g)}} p(Y, \mathcal{P}^{(g)}, \mathbf{x} | g, \Psi) d\mathcal{P} \quad (5)$$

As noted calculating (5) by pruning is intractable for DSMs. Instead we can approximate by Monte Carlo. The path representation has been used to sample $p(\Psi, \mathcal{P}^{(g)} | Y, g)$ using Markov chain Monte Carlo (MCMC) [32, 36, 2, 17], but approximating marginal likelihoods from MCMC samples is non-trivial [25, 1, 52], and determining MCMC runtimes difficult. A recent [28] importance sampling (IS) algorithm provides error bounds for approximating $p(\mathbf{y} | \mathbf{x}, t, \Psi_1)$ under DSMs via (4) with reweighted paths drawn from the ISM, and [29] improves these bounds using sequential Monte Carlo (SMC). Both methods require only samples from the ISM, enabling the use of existing phylogenetics software. Here we consider two methods that extend the approaches in [28, 29] to trees to enable Monte Carlo approximation of (5) under arbitrary DSMs. Both use *data augmentation importance sampling*, sampling the augmented space of paths to enable evaluation of importance weights. The relative performance of these approaches is compared in Section 5.

4.3 A stratified data augmentation importance sampler

Our first approach leverages bounded-error approximation of edge transition probabilities (4) [28] by rewriting (5) as a marginalization over sequences at internal nodes of g . Let $\mathbf{x} = (x_1, \dots, x_\ell)$ be the root UCA sequence and $Z = \{\mathbf{z}^1, \dots, \mathbf{z}^r\}$ internal node sequences $\mathbf{z}^i = (z_1^i, \dots, z_\ell^i)$, then

$$p(Y | g, \Psi) = \sum_{\mathbf{x}, Z} p(Y, Z, \mathbf{x} | g, \Psi) = \sum_{\mathbf{x}, Z} \int_{\mathcal{P}^{(g)}} p(Y, Z, \mathbf{x}, \mathcal{P}^{(g)} | g, \Psi) d\mathcal{P}, \quad (6)$$

$$= \sum_{\mathbf{x}, Z} p(Y, Z, \mathbf{x} | g, \Psi) \prod_{(\mathbf{u}, \mathbf{v}, t) \in E(g)} \int_{\mathcal{P}} p(\mathbf{v}, \mathcal{P}^{(t)} | \mathbf{u}, \Psi) d\mathcal{P} \quad (7)$$

with $E(g) := E(\mathbf{x}, Z, Y, g)$ the set of transitions along edges of g for observed sequences (\mathbf{x}, Z, Y) . The second line (7) follows from the Markov property of the evolutionary model.

Under an ISM, the marginal likelihood (6) of the tree g factors site by site, as shown in Figure 1b:

$$p_0(Y | g, \Psi_0) = \prod_{k=1}^{\ell} \sum_{x_k, Z_k} p(Y_k, Z_k, x_k | g, \Psi_0) \quad (8)$$

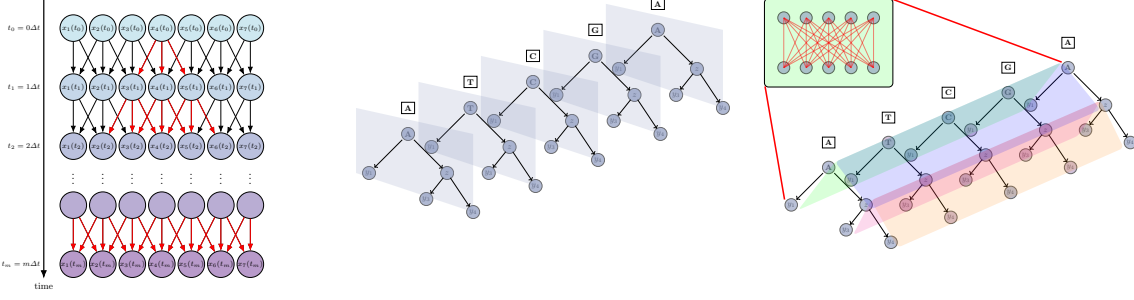


Fig. 1: Directed graphical models for site-dependent mutation. (a) Time-discretized CTMC with nearest-neighbor dependent rates. At each time t_j nucleotide $x_i(t_j)$ is conditionally dependent only on local sequence context $(x_{i-1}(t_{j-1}), x_i(t_{j-1}), x_{i+1}(t_{j-1}))$ at t_{j-1} , but this local dependence propagates recursively over time yielding long-range dependence after marginalizing intermediate sequences. In continuous time, each $x_i(t)$ depends on the entire sequence $\mathbf{x}(0)$ at every t . (b,c) Phylogenetic trees under independent- vs dependent-site mutation. Under independence (b) the model factors, and pruning can be performed at each site independently, but (c) under site dependence, nodes at each level become interdependent across all sites as in (a).

with the inner sum over nucleotides at site k of each unobserved sequence, and can be computed efficiently Felsenstein pruning [9], but computing (6) is intractable for DSMs where this factorization fails (Figure 1c).

The form (6) suggests a direct extension of the data augmentation importance sampler in [28] for approximating pairwise sequence transition probabilities under DSMs, to phylogenetic trees. Specifically, after sampling trees from the posterior distribution over genealogies under the independent site model:

$$g^{(j)} \sim \pi_0(g \mid Y, \Psi_0) \propto p_0(Y \mid g, \Psi_0) f_G(g) \quad j = 1, \dots, m \quad (9)$$

we wish to compute the *importance weights* $w(g^{(j)})$ under the DSM, defined by

$$w(g) := \frac{\pi_1(g \mid Y, \Psi_1)}{\pi_0(g \mid Y, \Psi_0)} \propto \frac{p_1(Y \mid g, \Psi_1)}{p_0(Y \mid g, \Psi_0)} = \sum_{\mathbf{x}} \frac{p_1(Y \mid \mathbf{x}, g, \Psi_1) p_1(\mathbf{x} \mid g, \Psi_1)}{p_0(Y \mid \mathbf{x}, g, \Psi_0) p_0(\mathbf{x} \mid g, \Psi_0)}, \quad (10)$$

in order to approximate posterior expectations under $\hat{\mathbb{E}}_{\pi_1}(h(g)) := \sum_{i=1}^m \tilde{w}(g^{(j)}) h(g^{(j)})$ for normalized weights \tilde{w} . Here $p_i(Y \mid g^{(j)}, \Psi_i)$ is the marginal likelihood of observed sequences Y for sampled tree $g^{(j)}$ under model $i = 0$ (ISM) or 1 (DSM). While factorization (8) enables efficient calculation of $p_0(Y \mid g, \Psi_0)$, exact computation of $p_1(Y \mid g, \Psi_1)$ is intractable. We instead approximate (10) itself by Monte Carlo integration. To simplify notation, we suppress conditioning on Ψ , and use p_0 and p_1 to distinguish the ISM and DSM.

A key to our approach is the factorization of the *complete data likelihood* into edge transition probabilities when (\mathbf{x}, Z) are observed: $p_i(Y, Z, \mathbf{x} \mid g) = p_i(\mathbf{x} \mid g) \prod_{(\mathbf{u}, \mathbf{v}, t) \in E} p_i(\mathbf{v} \mid \mathbf{u}, t)$, as seen in (7). Hence we can approximate (10) by sampling root and internal node sequences $(\mathbf{x}^{(i)}, Z^{(i)}) \sim p_0(\mathbf{x}, Z \mid Y, g)$ from the ISM conditional distribution via Felsenstein pruning [9] and forming the estimator

$$\hat{w}(g) = \frac{1}{m} \sum_{j=1}^m \frac{p_1(\mathbf{x}^{(j)} \mid g)}{p_0(\mathbf{x}^{(j)} \mid g)} \prod_{e \in E(Y, g, \mathbf{x}^{(j)}, Z^{(j)})} \hat{w}(e). \quad (11)$$

where \hat{w} is an unbiased estimator of the edge weight $\mathbb{E}(\hat{w}(e)) = w(e) := \frac{p_1(\mathbf{v} \mid \mathbf{u}, t)}{p_0(\mathbf{v} \mid \mathbf{u}, t)}$.

Estimating edge weights: Computing the ISM transition probability $p_0(\mathbf{v} \mid \mathbf{u}, t)$ (1) for edge $e = (\mathbf{u}, \mathbf{v}, t)$ is straightforward, but exact computation of $p_1(\mathbf{v} \mid \mathbf{u}, t)$ (3) remains intractable. [30, 29] give an unbiased estimator $\hat{w}(e)$ of $w(e)$ with bounded approximation error, using SMC. The SMC estimator uses a Gibbs sampler for sequence paths, which updates the path at each site conditional on the paths of its neighboring sites based on the context-dependent model (DSM). This SMC-based unbiased estimator takes the form

$$\hat{w}(e) = \prod_{s=1}^S \left(\frac{1}{n} \sum_{k=1}^n w_s(\mathcal{P}_s^{(k)}(e)) \right) := \prod_{s=1}^S \hat{w}_s(e) := \frac{\hat{p}_1(\mathbf{v} \mid \mathbf{u}, t)}{p_0(\mathbf{v} \mid \mathbf{u}, t)}, \quad (12)$$

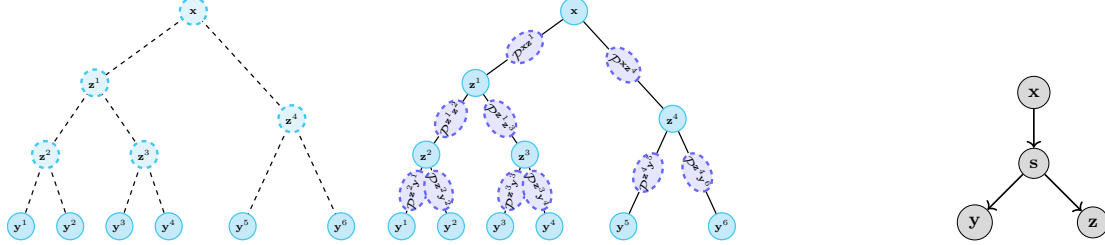


Fig. 2: (a,b) Schematic of two-stage (stratified) sampling procedure. (a) **Stage 1:** Latent internal node sequences ($\mathbf{x}, \mathbf{z}^{1:4}$) are sampled conditional on observed sequences ($\mathbf{y}^{1:6}$). Each sampled configuration defines a stratum. (b) **Stage 2:** Conditional on each configuration from Stage 1, the marginal transition probability for each edge (e.g. $p_1(\mathbf{z}^1 | \mathbf{x}, t_1)$) is approximated by endpoint-conditioned importance sampling of path. Given internal sequences, these transition probabilities are mutually independent. (c) A *star path* example.

where $\mathcal{P}^{(k)}(e)$ is the k th particle (evolutionary path from \mathbf{u} to \mathbf{v} in time t) for edge $e = (\mathbf{u}, \mathbf{v}, t)$, w_s the corresponding weight at the s th step, and n, S the numbers of particles and steps, respectively.

Estimating tree weights: Plugging (12) into (11), we obtain an estimator for $w(g)$:

$$\hat{w}(g) = \frac{1}{m} \sum_{j=1}^m \left(\frac{p_1(\mathbf{x}^{(j)} | g)}{p_0(\mathbf{x}^{(j)} | g)} \prod_{e \in E(Y, g, \mathbf{x}^{(j)}, Z^{(j)})} \prod_{s=1}^S \hat{w}_s(e) \right) := \frac{\hat{p}_1(Y, Z, \mathbf{x} | g)}{p_0(Y, Z, \mathbf{x} | g)} \quad (13)$$

for $\mathbf{x}^{(j)}$ and $Z^{(j)}$ sampled from $p_0(\mathbf{x}, Z | Y, g)$, their joint conditional posterior distribution under the ISM. The samples (9) from $\pi_0(g | Y)$ are readily available from standard Bayesian phylogenetics software packages [42]; our approach enables these to be extended to models with site-dependence. **Validation:** Table 1 shows this approach on an example small enough (6 sequences of length $\ell = 6$, Figure 3) for exact calculation via (3). Posterior probabilities of all trees are accurately approximated with a relatively small sample (2000); however, the effective sample size (ESS) varies significantly across trees. Trees with lower ESS values (e.g. #5) exhibit slightly larger errors, but not large enough to affect tree rankings.

Table 1: Exact vs approximated posterior prob. for 6 sequence example in Fig. 3

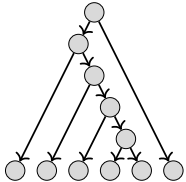


Fig. 3: True tree

Tree	Exact Value	IS	ESS	Tree	Exact Value	IS	ESS
#1	-32.837	-32.835	258.40	#6	-36.074	-36.025	63.57
#2	-34.193	-34.129	125.05	#7	-36.123	-36.092	386.44
#3	-34.642	-34.672	44.32	#8	-36.442	-36.262	210.98
#4	-34.869	-34.905	233.28	#9	-37.462	-37.335	285.60
#5	-35.121	-35.186	36.40	#10	-38.227	-38.256	116.26

4.4 Sequential Monte Carlo

To address the low ESS observed for some trees, we consider an alternative approximation of (6), by extending the SMC method of [29] from *sequence paths* to *tree paths* by introducing an MCMC sampler for the space $\mathcal{P}^{(Y, g)}$ of tree paths. The resulting method has similarities to the *stepping stone (StSt)* method [53]; but whereas the StSt method approximates likelihood ratios for alternate ISM substitution models using thermodynamic integration (TI) [10, 25], our approach evaluates DSM likelihoods using SMC via importance sampling identities, taking advantage of *exact* computability of $p_0(Y | g, \Psi_0)$ (8) given Ψ_0 . For notational simplicity, we assume the DSM is a *nearest-neighbor* model $\tilde{x}_i = (x_{i-1}, x_i, x_{i+1})$, but the method is general.

For a DSM (2), we define a sequence of intermediate models $\tilde{\gamma}_t(b; \tilde{x}) = \phi^t(b; \tilde{x})\gamma(b; x)$ on a temperature ladder $\mathcal{T} = \{0 = t_0 < t_1 < \dots < t_V = 1\}$. The SMC algorithm proceeds by:

1. *(Initialization)* Sample tree-path particles $\mathcal{P}_{0,1}^{(Y,g)}, \dots, \mathcal{P}_{0,N}^{(Y,g)} \stackrel{\text{iid}}{\sim} \pi_0(\cdot \mid Y, g)$ under the ISM, performed site-by-site by (i) sampling internal node sequences using Felsenstein pruning and then (2) sampling endpoint-conditioned substitution paths along each branch under the ISM [16, 37].
2. For $v = 1, \dots, V$:
 - (i) *(Resampling)* Sample $\tilde{\mathcal{P}}_{v,1}^{(Y,g)}, \dots, \tilde{\mathcal{P}}_{v,N}^{(Y,g)}$ with probability $\propto w_v(\mathcal{P}_{v-1}^{(Y,g)}) := \frac{p_{t_v}(Y, \mathcal{P}_{v-1,i}^{(Y,g)} \mid g)}{p_{t_{v-1}}(Y, \mathcal{P}_{v-1,i}^{(Y,g)} \mid g)}$.
 - (ii) *(Mutation)* Sample $\mathcal{P}_{v,1}^{(Y,g)}, \dots, \mathcal{P}_{v,N}^{(Y,g)}$ where $\mathcal{P}_{v,i}^{(Y,g)} \mid \tilde{\mathcal{P}}_{v,i}^{(Y,g)} \sim \mathbf{K}_v^s(\tilde{\mathcal{P}}_{v,i}^{(Y,g)}, \cdot)$ and \mathbf{K}_v is an ergodic π_{t_v} -invariant Markov kernel.
3. Form the estimate $\hat{p}_1(Y \mid g) = p_0(Y \mid g) \prod_{v=1}^V \frac{1}{N} \sum_{i=1}^N w_v(\mathcal{P}_{v-1,i}^{(Y,g)})$. (14)

Step 2(i) describes multinomial resampling for simplicity of presentation; in practice alternative variance-reduction techniques are preferred for resampling [7]. Step 2(ii) is implemented by simulating the evolution of each particle according to the Markov kernel K_v for s steps. We therefore require a π_{t_v} -invariant Markov kernel, which we now construct. Specifically, we extend the MCMC kernel of [26] for pairwise endpoint-conditioned sequence paths to a MCMC kernel on tree-paths. The pairwise kernel is a Metropolis–Hastings chain using the Hobolth algorithm [15] as a proposal distribution (see Appendix for additional details).

Star-path MCMC kernel: We introduce a Markov kernel on tree-path space that updates tree-paths component-wise by (randomly or systematically) selecting a tree node \mathbf{s} and proposing a *star-path* change; see Figure 2 (each of the four nodes represents a sequence of length ℓ). Let $\mathbf{s}_{-i} = \{s_1, \dots, s_{i-1}, s_{i+1}, \dots, s_\ell\}$, and let $\mathcal{P}^{(\mathbf{xs})} := (\mathcal{P}_1^{(\mathbf{xs})}, \dots, \mathcal{P}_\ell^{(\mathbf{xs})})$ be an evolutionary path from \mathbf{x} to \mathbf{s} with $\mathcal{P}_j^{(\mathbf{xs})}$ the path at site j from x_j to s_j . The kernel draws a *single-site star-path* $\mathcal{P}_i^{(\mathbf{xsyz})} := (\mathcal{P}_i^{(\mathbf{xs})}, \mathcal{P}_i^{(\mathbf{sy})}, \mathcal{P}_i^{(\mathbf{sz})})$ conditional on paths at all other sites, i.e. $p_1(\mathcal{P}_i^{(\mathbf{xsyz})} \mid \mathcal{P}_{[-i]}^{(\mathbf{xsyz})})$. A detailed description of this MCMC procedure is given in Appendix C.

4.5 Comparison

Table 2 compares Stratified Sampling (13), Importance Sampling, and SMC (14) for equal particle numbers, and for equal computational budget. The results show marked differences: SMC consistently surpasses SS and IS, achieving substantially higher ESS (≥ 971.71 /step with 1024 particles) in both scenarios, two orders of magnitude greater than either SS or IS. Under equal computational budgets, the simplicity of IS allows higher throughput (2.56×10^6 particles (ESS 137.33) to SMC’s 1024), but SS manages only a $4\times$ increase and little ESS improvement. The surprisingly dominant performance of SMC can be explained by more efficient allocation of samples in (\mathbf{x}, Z) space by the MCMC chain relative to the ISM proposal; see Appendix E.

Fixed Particle Count		Fixed Computational Budget			
Method	Particles (N)	ESS	Method	Particles (N)	ESS
SS	1,024	1.11	SS	4,096	1.22
IS	1,024	4.88	IS	2,560,000	137.33
SMC	1,024	≥ 971.71	SMC	1,024	≥ 971.71

Table 2: Effective sample sizes for importance sampling (IS), stratified IS (SS), and sequential Monte Carlo (SMC) estimators of posterior probability under the ARMADiLLO model, for a phylogenetic tree of the DH270 clone sampled by `linearham`. ESS for SMC is per step. Under fixed computational budget, all algorithms were run for the same CPU time required for SMC.

4.6 Incorporating VDJ Model-Based Priors on the UCA

Most applications of phylogenetic inference assume the common ancestor \mathbf{x} is drawn from the stationary distribution of the evolutionary model. However, solving for the stationary distribution of a CTMC model with arbitrary site-dependence can be difficult, with the chain often non-reversible. (An exception is if the model satisfies conditions guaranteeing the stationary distribution is a Markov random field;

see [22].) For reconstructing BCR lineages, this assumption is not appropriate: the UCA is generated by VDJ recombination of germline sequences. Stochastic models of VDJ recombination are well-established [8, 34], and these models can provide informative prior distributions on the UCA during BCR lineage reconstruction [35, 6]. Prior distributions on the UCA can be incorporated into the importance sampling approaches of Sections 4.3 and 4.4. Let $\zeta_0(\mathbf{x})$ denote the marginal distribution of \mathbf{x} in the importance sampling proposal (e.g. the stationary distribution under ISM p_0), and $\zeta_1(\mathbf{x})$ the desired prior, then we have $p_i(Y, \mathbf{x}, Z | g) = \zeta_i(\mathbf{x}) \prod_{(\mathbf{u}, \mathbf{v}, t) \in E(g, \mathbf{x}, Z, Y)} p_i(\mathbf{v} | \mathbf{u}, t)$ and the importance weights can be calculated as before. However, for the VDJ model these priors may place mass on significantly different sequences, leading to inflation of importance weights. To prevent this, we instead we use the approach of [6] to sample from the posterior defined by the VDJ model combined with the ISM model for SHM: $\pi_{0, \text{VDJ}} \propto p_0(Y, Z | \mathbf{x}, g) \zeta_{\text{VDJ}}(\mathbf{x})$. In this case the prior ζ_{VDJ} cancels out of the importance weights, and the estimator (13) remains unchanged.

Piecewise VDJ prior: In Section 5, we show that the VDJ prior improves reconstruction on germline-encoded regions, but sometimes causes errors in non-templated regions. We therefore define a piecewise prior under which the VDJ model applies outside the CDR3 region but *not* within the CDR3 itself. To draw from the posterior we use `linearham` [6] to sample $\pi_{0, \text{VDJ}}$ then substitute a CDR3 drawn from $p_0(\mathbf{x}_{\text{CDR3}} | Y, g)$ by pruning, resulting in the piecewise prior $p_{\text{VDJ}}(\mathbf{x}_{\overline{\text{CDR3}}} \zeta_0(\mathbf{x}_{\text{CDR3}})$, and the weight (10) remains correct.

4.7 Bayes Estimators for the UCA

Bayesian inference results in a posterior distribution $\pi_1(\mathbf{x}, g | Y)$, but users often prefer to obtain a single reconstructed lineage g or UCA \mathbf{x} , requiring summarization of the posterior π_1 by a point estimate. To evaluate reconstruction accuracy we consider the *maximum a posteriori* (MAP) estimator $\hat{\mathbf{x}}_{\text{MAP}}$ defined by the sampled UCA with highest estimated posterior probability and the *marginal mode* (MM) estimator $\hat{\mathbf{x}}_{\text{MM}}$ which concatenates the nucleotides maximizing the marginal posteriors at each sequence position; explicit formulas for these estimators are given in Appendix D.

5 Results

We first describe experiments on simulated datasets designed to demonstrate the effectiveness of our approach, and to investigate impact of accounting for context-dependence on the reconstruction of phylogenetic trees (B cell lineages) and ancestral sequences (UCAs). We then apply our approach to the analysis of BCR repertoires for two important broadly-neutralizing HIV antibodies DH270 and CH235.

In each case, inference is performed according to the importance sampling approaches of Section 4. Samples from the posterior distribution of trees under the pure phylogenetic ISM were generated using Beast [42] under a Yule process tree prior and assuming the strict clock model. Inference was performed using two MCMC chains with 10M iterations each, with a burn-in of 6M and thinning of 1k. Convergence was diagnosed by the ESS (as reported by Beast) for both the joint probability under the ISM and the root height of trees, so the number of root and internal node sequence samples varies by problem.

5.1 Simulation study design

To evaluate the accuracy of our approach on data for which the ground truth (genealogy and UCA) are known, we simulated multiple sets of BCR sequences, each representing a clonal repertoire dataset. Sequences were simulated using a neutrally evolving branching process consisting of a $\text{Pois}(\lambda)$ progeny distribution and a $\text{Pois}(\lambda_{\text{len}})$ branch length generating distribution [5], starting from a single naive sequence (the UCA). The number of progeny cells is determined by a $\text{Pois}(\lambda)$ draw: zero means the cell dies, one means no division, and two or more means the cell splits. Each progeny cell then undergoes evolution for a time interval drawn from $\text{Pois}(\lambda_{\text{len}})$, with somatic hypermutations occurring sequentially and incorporating context-sensitivity. The simulation concludes when all cells die or a pre-determined time is reached [5]. In what follows, we set $\lambda = 1.5$ and $\lambda_{\text{length}} = 0.005$, similar to real SHM rates [5].

5.2 Effects of context-dependence on tree and UCA reconstruction accuracy

Short Sequences: CDR3 regions The complementarity-determining region 3 (CDR3) of antibodies is a region of high variability that plays a crucial role in antigen recognition and binding. Therefore, we first focus on short sequences simulated from the CDR3 of a bnAb UCA. Two independent (tree, clonal sequence repertoire) sets were simulated. Samples from the posterior distribution over trees under the pure phylogenetic ISM model were obtained using Beast, and posterior probabilities under the DSM calculated from importance weights (13). Results for UCA reconstruction are summarized in Table 3a. The DSM consistently outperforms the ISM for all estimators. Also shown are UCAs reconstructed conditional on the true tree (unknown in practice); unsurprisingly, this significantly reduces UCA reconstruction error, but moreso for the ISM. Thus a key role of the DSM appears to be in improving the estimated tree.

Full length BCR sequences Next we simulated 8 independent (tree, clonal sequence repertoire) sets of full length BCR sequences from an estimated UCA for HIV bnAb CH235. Each tree was pruned to select a subset of nodes to match individual Hamming distances of a real BCR dataset while ensuring no selected node was an ancestor/descendant of another, to approximate fixed-depth sequencing of BCR repertoires. Reconstruction accuracy is shown in Table 3a. In each simulated dataset, the true tree ranks as the highest probability under the DSM. For these longer sequences the number of reconstruction errors is larger, and the improvement obtained under the DSM is even clearer. (In Table 3 ISM refers to the mean-field DSM approximation (see Appdx F); SHM to the pure phylogenetic model; VDJ to Linearham. IgPhyml does not do CDR3 junction inference [18] so does not provide a meaningful comparison.)

Improving UCA reconstruction with VDJ recombination models: In standard phylogenetics, the common ancestor \mathbf{x} is assumed to be drawn from the stationary distribution of the evolutionary model. In affinity maturation, the UCA is generated by the mechanisms of VDJ recombination. [19, 46]. Detailed stochastic models of this process have been developed [6, 23, 27] that assign a probability to every possible UCA sequence arising from the host germline VDJ gene segment library via recombination and n -nucleotide insertion. Although developed for BCR sequence analysis including the specific purpose of lineage reconstruction and UCA estimation, these models have relied primarily on independent-site models of SHM. However, VDJ models can provide additional information regarding the UCA prior to SHM, and incorporating this information may be expected to improve reconstruction accuracy. Table 3a shows the results of incorporating the HMM-based VDJ rearrangement model of [6]. As expected, the accuracy of UCA reconstruction does indeed significantly improve, although accuracy obtained by our importance sampling-based DSM estimator is constrained by the failure of the ISM-based `linearham` model to sample the correct UCA at all. Notably, all observed reconstruction errors occur in the CDR3 region, suggesting that the prior information of the VDJ model significantly improves accuracy in the germline-templated V, and J regions, but is less accurate in the highly variable n -nucleotide inserted regions, where it may actually introduce errors. **Piecewise VDJ prior:** Table 3a shows that substituting the piecewise prior described in section 4.6 for the full VDJ prior does indeed provide a small further improvement in UCA reconstruction accuracy.

VDJ Reparameterization: Results in Table 3a incorporating the VDJ prior were obtained using default parameters for `linearham`. To test the sensitivity of these results to the parameterization of the VDJ model, we re-ran simulation studies using a parameter set for `linearham` obtained by training on a large NGS dataset of human B cell repertoire heavy chain sequences. 10 independent simulated clonal datasets were generated using UCAs sampled from the stochastic VDJ rearrangement process (via `linearham`) and a tree topology (including branch lengths) sampled from the Yule prior. Observed sequences were then obtained by simulating context-dependent evolution under the ARMANDILLO model along the sampled tree topology. These simulated repertoires match many key statistics of real-world clones, with a typical clone having sequence length around 365 and containing 55 highly-mutated observed sequences, with average Hamming distance from the UCA of 84.44 ($\approx 75\%$ sequence identity), average tree depth similar to that of trees reconstructed for the CH235 clone, and depth of the leaf closest to the root (which provides most information about the UCA) of 0.08 with 27.35 mutations from the root sequence on average (least mutated sequence in real CH235 clone dataset: 27 mutations). SMC was used in all reconstructions based on results in Table 2.

Dataset	CDR3		Full Length BCR (SS)					
Model	SHM		SHM		+VDJ		+piecewise	
CDR3	Yes	Yes	No	Yes	No	Yes	No	
Estimator	T	T_{MAP}	T^*	\bar{T}	T	T	T	T
$\hat{\mathbb{E}}_{p_0}[d(\cdot, \mathbf{x}^*)]$	6.6	6.0	1.2	1.2	16.5	3.2	0	2.4
$\hat{\mathbb{E}}_{p_1}[d(\cdot, \mathbf{x}^*)]$	4.9	5.3	1.0	1.0	13.9	3.0	0	1.9
$\text{UCA}_{\text{ISM}}^{\text{MAP}}$	6	7	1	1	16	3	0	2
$\text{UCA}_{\text{ISM}}^{\text{MM}}$	7	7	1	1	13	3	0	2
$\text{UCA}_{\text{DSM}}^{\text{MAP}}$	5	5	1	1	12	2	0	1
$\text{UCA}_{\text{DSM}}^{\text{MM}}$	5	5	1	1	11	2	0	1
								0

	Full Length BCR (SMC), with NGS-VDJ			
	ISM	DSM	mean diff. [range]	% of UR
$\hat{\mathbb{E}}[d(\cdot, \mathbf{x}^*)]$	3.5	2.0	1.45 [0.25, 2.63]	4.8%
$d(\hat{\mathbf{x}}_{\text{MM}}, \mathbf{x}^*)$	2.6	2.2	0.40 [0, 2]	1.3%
$d(\hat{\mathbf{x}}_{\text{MAP}}, \mathbf{x}^*)$	2.8	2.2	0.60 [0, 2]	2.0%
	ISM g^*	DSM g^*	mean diff. [range]	% of UR
$\hat{\mathbb{E}}[d(\cdot, \mathbf{x}^*)]$	2.4	2.0	0.39 [-0.20, 0.93]	1.3%
$d(\hat{\mathbf{x}}_{\text{MM}}, \mathbf{x}^*)$	2.4	1.8	0.60 [0, 1]	2.0%
$d(\hat{\mathbf{x}}_{\text{MAP}}, \mathbf{x}^*)$	2.4	1.8	0.60 [0, 1]	2.0%

Table 3: (a) Hamming distance between estimated and true UCA \mathbf{x}^* , for various models and estimators described in text. \bar{T} denotes marginalization over the posterior distribution on trees; T_{MAP} and T^* denote conditioning on the MAP and true trees, respectively. Errors are divided into CDR3 and non-CDR3 regions. (b) Hamming distance using SMC algorithm and NGS-retrained VDJ model, averaged over 10 independent simulations. Differences show improvement of DSM over ISM in terms of sites and as % of uncertain region (UR) consisting of N-nucleotides and D gene segments (average length: 30). Differences occur at a small fraction of sequence positions, but ISM errors are at functionally critical sites (Sec. 5.3).

Table 3b shows the resulting DSM error rate is 6.6% versus 11.6% for the ISM, a reduction of 43.1%. The retrained VDJ prior no longer induces errors in the CDR3. (However, most users will not have access to a large application-specific NGS dataset to retrain `linearham`, so we still recommend the piecewise prior for robustness as in Table 3a.) Again a major source of error in UCA reconstruction comes from inaccuracies in the inferred tree; the DSM is able to more accurately reconstruct the tree, which in turn leads to improved accuracy in the UCA reconstruction. Figure 4a shows estimated marginal probability of UCA reconstruction errors by site for one simulated clone, demonstrating the significant improvement under the DSM. Figure 4b,c

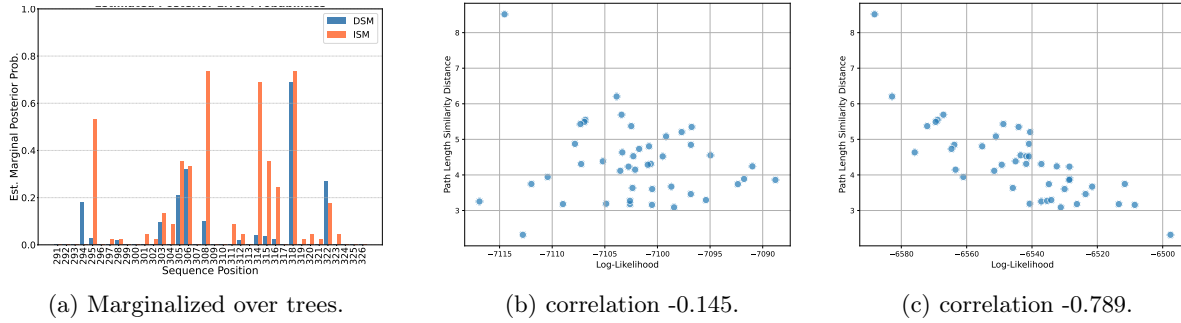


Fig. 4: (a) Marginal probability of reconstruction error by UCA position under ISM vs DSM. The DSM shows reduced errors at all positions except bases 294 and 322. Most errors occur in positions 314, 315, and 316 that have neighboring mutations which are more accurately reconstructed by accounting for context-dependence. (b,c) Tree likelihood vs. (path length similarity) distance from true tree, under (b) ISM and (c) DSM. Posterior mean distance is 3.89 (ISM) and 2.31 (DSM). The sampled tree with smallest plsd to the true tree ranks 3rd-to-last under the ISM among all sampled trees, but 1st (most probable) under the DSM.

shows log-likelihood of trees versus distance to the true tree for both the ISM and DSM using path length similarity distance [51, 40], chosen due to vaccinologists' emphasis on the temporal trajectory of antibody lineages. Log-likelihoods under the DSM correlate more strongly with proximity to the true tree.

Observed ISM mistakes To understand the impact of the independent site assumption in the presence of site-dependence, we identified mistakes commonly observed under ISM reconstruction. These illustrate how failure to account for context-dependent mutation leads to inaccuracies in phylogenetic tree reconstruction.

Scenario 1: Figure 5a shows a small subtree of a larger tree, with S_{1560} , S_{1561} and S_{4211} observed leaves. It thus represents a tree reconstruction problem with only 3 leaf nodes and observed sequences of length 367. Despite the large amount of information, the ISM-reconstructed topology is incorrect. Under the ISM, the reconstructed tree minimizes the sum of Hamming distances along edges. Key sites are 147 and 188: Figure 5 shows that S_{1561} and S_{4211} agree on T at site 146 while S_{1560} and S_{4211} agree on C at site 188, hence the ISM estimates the UCA as T at site 147 and C at site 188 with high probability, ensuring each site has only experienced a single mutation. However the DSM assigns a lower probability to the ISM tree since these two key mutations occur in highly mutable motifs. As seen in Figure 5b, the ISM tree requires site 147 to remain unmutated along the path $E \rightarrow F \rightarrow S_{1561}$ and the path $E \rightarrow F \rightarrow S_{4211}$, which is far less likely under the DSM.

Scenario 2: In the example of Figure 5d, the (sub)tree obtained under the ISM has Hamming distance 8 between the UCA (node A) and S_{80} . Since 4 of those 8 mutations are shared with S_{245} , the ISM places S_{80} and S_{245} on the same lineage $A \rightarrow D$. However, the contexts of these 4 mutations are highly mutable, and under the DSM they are more likely to have been duplicated independently along separate lineages.

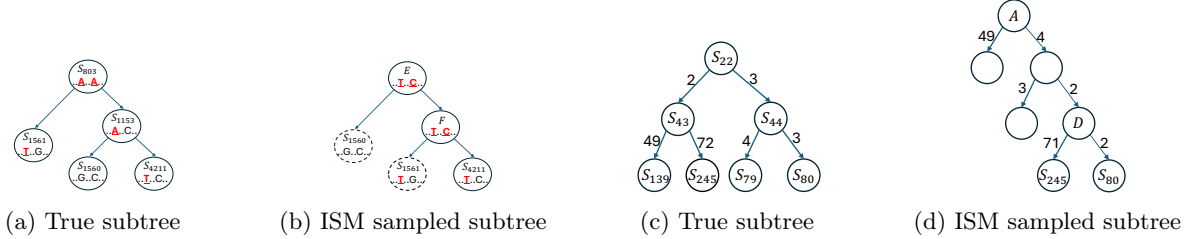


Fig. 5: Errors in ISM tree reconstruction. (a,b) The ISM essentially reconstructs the root sequence by finding common bases, but highly mutable bases (red) in the UCA are less conserved at leaves, and finding common bases can fail. (Dashed circles show mistakes in inferred tree.) (c,d) The 4 of the 8 mutations along $A \rightarrow D$ that are shared by S_{245} and S_{80} are highly mutable under the DSM.

5.3 Analysis of HIV bnAb B cell repertoires

We applied our method to infer the UCA and lineage tree of two well-characterized HIV bnAb clones, CH235 and DH270 which have served as prototypical examples of bnAb maturation as well as templates for lineage-based HIV vaccine design [4, 3, 38, 50]. The DH270 clonal lineage tree was reconstructed using heavy chain sequences of 6 observed members and the CH235 clonal lineage was reconstructed using heavy chain sequences of 55 observed members. The limited number of observed sequences in the DH270 clone and the extensive diversity of CDRH3 sequences observed in the CH235 clone (see Figure S2 in Appendix) make these clones particularly challenging test cases for accurate clonal tree reconstruction.

DH270 The UCA estimated for the DH270 clone under the DSM differs by only a single amino acid from the UCA estimated under the ISM, in 7th position of CDRH3 (Fig. 6a, red). This site, which is reconstructed as a glycine under the ISM and a serine under the context-dependent model, occurs unambiguously in the non-templated nucleotide (n-nucleotide) regions that are not encoded by the V, D or J gene segments and thus cannot be resolved by priors on the initial VDJ rearrangement. While this difference in reconstructions would appear to be small, in fact the 7th position in the CDRH3 is critical for binding of DH270 lineage members to the HIV Env protein as it makes structural contacts to the V3 glycan epitope [14]. Moreover, deep scanning mutagenesis in the CDRH3 of a previously inferred DH270 UCA revealed that the 7th position in the CDRH3 could only tolerate a serine to maintain binding to the designed priming immunogen [43]. Thus, the one position difference between the ISM and DSM reconstructions occurs at a key site for both bnAb epitope recognition and for binding to an immunogen designed to activate the DH270 lineage, and represents a critical error of the ISM assumption. This example underscores the importance of highly accurate UCA

estimates for both understanding the natural maturation history of clonal lineages and for vaccine design. While the true UCA sequence for the DH270 clone is unknowable, the fact that the DSM-estimated UCA contains the serine at this critical 7th position which is the only amino acid compatible with binding to the designed priming immunogen – itself a modified form of an HIV Env circulating at the time the DH270 clone emerged – suggests that the DSM-estimated UCA may more accurately reflect the true ancestral sequence. Moreover, designing an immunogen to elicit this bnAb based on the incorrect ISM-reconstructed UCA could be counterproductive, potentially selecting for mutants that compete *against* the desired bnAb.

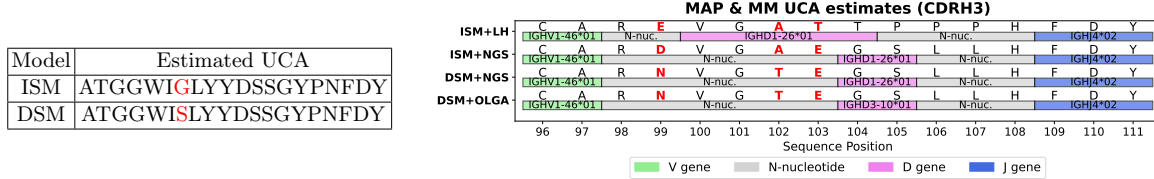


Fig. 6: MAP UCA estimates for HIV bnAb DH270 and CH235 clones (displaying only CDR3 region). Shown are independent site model with VDJ prior using Linearham with (ISM+LH) default parameters, vs. (ISM+NGS) parameters from a large human B cell NGS dataset; and context-dependent model with (DSM+NGS) Linearham VDJ prior with NGS parameters, vs. (DSM+OLGA) OLGA [39] VDJ prior.

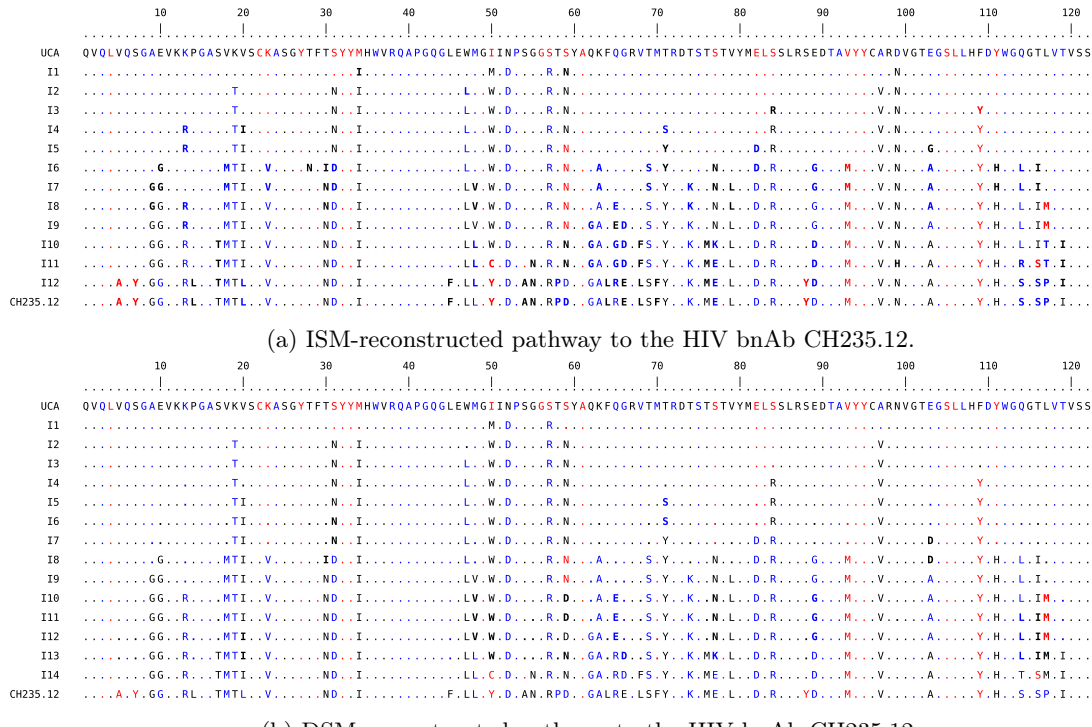


Fig. 7: Reconstructed mutational pathways to an HIV bnAb. (Trees shown in Figure AS3b.) Red/blue indicates hot/cold spots in the codon, while bold characters highlight differing estimates between the models.

CH235 We observe two amino acid differences between the ISM and DSM reconstructions of the CH235 UCA CDRH3, at positions 99 and 102 (Fig. 6b). The CH235 CDRH3 forms extensive structural contacts with

the epitope and is critical for recognition of the conserved CD4 binding site [13]. Position 102 makes direct contact with the CH235 epitope, and position 99 likely influences CDRH3 positioning which may be critical for epitope recognition. This underscores the importance of accurate inference of the unmutated CDRH3 in order to identify Env variants capable of engaging CH235 precursor B cells, a key step in immunogen design.

Understanding the order in which critical mutations are acquired by bnAbs while developing neutralization breadth is also important for understanding how bnAb B cells mature during infection, and can inform vaccine strategies aiming to induce similar evolutionary trajectories in vaccinees [50]. Accurate estimates of internal nodes in the clonal lineage tree are therefore also important. Observed differences in the reconstructed topologies under the DSM and ISM (Figure S3) indicate that the tree reconstruction is heavily influenced by the choice of model, with the MAP trees showing key differences in mutational orderings (Figures 7 & S3), including differences in estimated acquisition timing 3 of mutations critical for bnAb epitope recognition. In the DSM tree, the W47L mutation which is critical for broad neutralization but highly improbable [49], emerges later in the maturation pathway, suggesting it requires prolonged clonal residence in the germinal center to arise. Another mutation S59N, which contacts the Env V5 loop in the CD4 binding site, is also estimated to occur later in the DSM vs. ISM MAP trees. These findings have implications for vaccine regimen design, as sequential boosting immunogens targeting key mutations may need to be timed carefully as boosting too early could misdirect maturation from its natural trajectory. The ISM tree also displays three amino acid transitions at contact position 65 (Q→E→G→R), whereas the DSM tree displays only two (Q→E→R), indicating that context-aware estimates can lead to more parsimonious lineages at critical positions. Together, these differences underscore the importance of modeling context-dependence in obtaining accurate inferences on the ordering and timing of mutations, both for understanding how B cells evolve and for designing vaccine strategies that aim to guide B cell maturation.

6 Discussion

The algorithms introduced here enable practical reconstruction of B cell lineages and UCAs under context-dependent models of somatic hypermutation such as ARMADILLO. Our results demonstrate that ignoring this context dependence, as all existing B cell lineage reconstruction methods do to our knowledge, introduces errors that may have important impacts on lineage-based vaccine design. We note that our comparisons on simulated and real data show differences between ISM- and DSM-reconstructed UCAs at only a few sites. This is because (a) existing VDJ models recover the (germline-encoded) majority of the BCR sequence with high accuracy, and (b) for moderate-to-large clones, consensus reconstruction suffices for most n -nucleotide insertion sites. However, reconstruction of tree topology and mutation ordering appears to be harder – and more sensitive to context dependence – than UCA reconstruction, with the DSM performing significantly better (Fig. 4b,4c), and UCA differences are often attributable to the ISM getting the tree partially wrong. For the HIV bnAb clones analyzed the UCA differences, while few, are functionally critical, while the observed differences in mutation ordering have real consequences for vaccine design.

Both the SS and SMC algorithms described here are highly parallelizable. The SMC approach is currently preferred due to the high variance of importance weights observed for SS; as described in Appdx E this is due to the sampled (\mathbf{x}, Z) distribution. We are currently exploring whether sampling from improved approximations to $\pi_1(\mathbf{x}, Z \mid Y, g)$ based on pruning with truncated dependence can make this method competitive with SMC. Another significant limitation of our importance-sampling approach is that we currently only evaluate $\pi_1(g \mid Y)$ for trees drawn from $\pi_0(g \mid Y)$. Supplementing sampled trees by performing a local search around large weight trees (e.g. [48]) may further improve topology exploration.

References

1. Arima, S., Tardella, L.: Improved harmonic mean estimator for phylogenetic model evidence. *Journal of Computational Biology* **19**(4), 418–438 (2012)
2. Bollback, J.P.: SIMMAP: Stochastic character mapping of discrete traits on phylogenies. *BMC Bioinformatics* **7**(1), 88 (2006)
3. Bonsignori, M., Kreider, E.F., Fera, D., Meyerhoff, R.R., Bradley, T., Wiehe, K., Alam, S.M., Aussedat, B., Walkowicz, W.E., Hwang, K.K., Saunders, K.O., Zhang, R., Gladden, M.A., Monroe, A., Kumar, A., Xia, S.M., Cooper, M., Louder, M.K., McKee, K., Bailer, R.T., Pier, B.W., Jette, C.A., Kelsoe, G., Williams, W.B., Morris, L., Kappes, J., Wagh, K., Kamanga, G., Cohen, M.S., Hraber, P.T., Montefiori, D.C., Trama, A., Liao, H.X., Kepler, T.B., Moody, M.A., Gao, F., Danishefsky, S.J., Mascola, J.R., Shaw, G.M., Hahn, B.H., Harrison, S.C., Korber, B.T., Haynes, B.F.: Staged induction of HIV-1 glycan-dependent broadly neutralizing antibodies. *Sci Transl Med* **9**(381) (2017)
4. Bonsignori, M., Zhou, T., Sheng, Z., Chen, L., Gao, F., Joyce, M.G., Ozorowski, G., Chuang, G.Y., Schramm, C.A., Wiehe, K., Alam, S.M., Bradley, T., Gladden, M.A., Hwang, K.K., Iyengar, S., Kumar, A., Lu, X., Luo, K., Mangiapani, M.C., Parks, R.J., Song, H., Acharya, P., Bailer, R.T., Cao, A., Druz, A., Georgiev, I.S., Kwon, Y.D., Louder, M.K., Zhang, B., Zheng, A., Hill, B.J., Kong, R., Soto, C., Mullikin, J.C., Douek, D.C., Montefiori, D.C., Moody, M.A., Shaw, G.M., Hahn, B.H., Kelsoe, G., Hraber, P.T., Korber, B.T., Boyd, S.D., Fire, A.Z., Kepler, T.B., Shapiro, L., Ward, A.B., Mascola, J.R., Liao, H.X., Kwong, P.D., Haynes, B.F.: Maturation pathway from germline to broad HIV-1 neutralizer of a CD4-mimic antibody. *Cell* **165**(2), 449–463 (2016)
5. Davidsen, K., Matsen, F.A.: Benchmarking tree and ancestral sequence inference for B cell receptor sequences. *Frontiers in Immunology* **9** (2018)
6. Dhar, A., Ralph, D.K., Minin, V.N., Matsen, IV, F.A.: A Bayesian phylogenetic hidden Markov model for B cell receptor sequence analysis. *PLOS Computational Biology* **16**(8), 1–27 (2020)
7. Doucet, A., de Freitas, N., Gordon, N.: *Sequential Monte Carlo Methods in Practice*. Springer, New York (2001)
8. Elhanati, Y., Sethna, Z., Marcou, Q., Callan, C.G., Mora, T., Walczak, A.M.: Inferring processes underlying B-cell repertoire diversity. *Philosophical Transactions of the Royal Society B: Biological Sciences* **370**(1676), 20140243 (2015)
9. Felsenstein, J.: Evolutionary trees from DNA sequences: A maximum likelihood approach. *Journal of Molecular Evolution* **17**(6), 368–376 (1981)
10. Gelman, A., Meng, X.L.: Simulating normalizing constants: From importance sampling to bridge sampling to path sampling. *Statistical Science* **13**(2), 163–185 (1998), publisher: Institute of Mathematical Statistics
11. Haynes, B.F., Kelsoe, G., Harrison, S.C., Kepler, T.B.: B-cell-lineage immunogen design in vaccine development with HIV-1 as a case study. *Nat Biotechnol* **30**(5), 423–33 (2012)
12. Haynes, B.F., Wiehe, K., Borrow, P., Saunders, K.O., Korber, B., Wagh, K., McMichael, A.J., Kelsoe, G., Hahn, B.H., Alt, F., Shaw, G.M.: Strategies for HIV-1 vaccines that induce broadly neutralizing antibodies. *Nat Rev Immunol* (2022)
13. Henderson, R., Anasti, K., Manne, K., Stalls, V., Saunders, C., Bililign, Y., Williams, A., Bubphamala, P., Montani, M., Kachhap, S., Li, J., Jaing, C., Newman, A., Cain, D.W., Lu, X., Venkatayogi, S., Berry, M., Wagh, K., Korber, B., Saunders, K.O., Tian, M., Alt, F., Wiehe, K., Acharya, P., Alam, S.M., Haynes, B.F.: Engineering immunogens that select for specific mutations in HIV broadly neutralizing antibodies. *Nat. Commun.* **15**(1), 9503 (2024)
14. Henderson, R., Zhou, Y., Stalls, V., Wiehe, K., Saunders, K.O., Wagh, K., Anasti, K., Barr, M., Parks, R., Alam, S.M., Korber, B., Haynes, B.F., Bartesaghi, A., Acharya, P.: Structural basis for breadth development in the HIV-1 V3-glycan targeting DH270 antibody clonal lineage. *Nat. Commun.* **14**(1), 2782 (2023)
15. Hobolth, A.: A Markov chain Monte Carlo expectation maximization algorithm for statistical analysis of DNA sequence evolution with neighbor-dependent substitution rates. *Journal of Computational and Graphical Statistics* **17**(1), 138–162 (2008)
16. Hobolth, A., Stone, E.A.: Simulation from endpoint-conditioned, continuous-time Markov chains on a finite state space, with applications to molecular evolution. *The Annals of Applied Statistics* **3**(3), 1204 – 1231 (2009)
17. Hobolth, A., Thorne, J.L.: Sampling and summary statistics of endpoint-conditioned paths in DNA sequence evolution. *Bayesian phylogenetics: methods, algorithms, and applications*. Chapman and Hall/CRC (2014)
18. Hoehn, K.B., Heiden, J.A.V., Zhou, J.Q., Lunter, G., Pybus, O.G., Kleinsteine, S.H.: Repertoire-wide phylogenetic models of B cell molecular evolution reveal evolutionary signatures of aging and vaccination. *Proceedings of the National Academy of Sciences* **116**(45), 22664–22672 (2019)
19. Hozumi, N., Tonegawa, S.: Evidence for somatic rearrangement of immunoglobulin genes coding for variable and constant regions. *Proceedings of the National Academy of Sciences* **73**(10), 3628–3632 (1976)
20. Jardine, J.G., Kulp, D.W., Havenar-Daughton, C., Sarkar, A., Briney, B., Sok, D., Sesterhenn, F., Ereno-Orbea, J., Kalyuzhniy, O., Deresa, I., Hu, X., Spencer, S., Jones, M., Georges, E., Adachi, Y., Kubitz, M., deCamp,

A.C., Julien, J.P., Wilson, I.A., Burton, D.R., Crotty, S., Schief, W.R.: HIV-1 broadly neutralizing antibody precursor B cells revealed by germline-targeting immunogen. *Science* **351**(6280), 1458–63 (2016)

21. Jardine, J.G., Ota, T., Sok, D., Pauthner, M., Kulp, D.W., Kalyuzhniy, O., Skog, P.D., Thinnes, T.C., Bhullar, D., Briney, B., Menis, S., Jones, M., Kubitz, M., Spencer, S., Adachi, Y., Burton, D.R., Schief, W.R., Nemazee, D.: HIV-1 vaccines. Priming a broadly neutralizing antibody response to HIV-1 using a germline-targeting immunogen. *Science* **349**(6244), 156–61 (2015)
22. Jensen, J.L., Pedersen, A.M.K.: Probabilistic models of DNA sequence evolution with context dependent rates of substitution. *Advances in Applied Probability* **32**(2), 499–517 (2000), publisher: Applied Probability Trust
23. Kepler, T.: Reconstructing a B-cell clonal lineage. I. Statistical inference of unobserved ancestors. *F1000Research* **2**(103) (2013)
24. Kwong, P.D., Mascola, J.R.: HIV-1 vaccines based on antibody identification, B cell ontogeny, and epitope structure. *Immunity* **48**(5), 855–871 (2018)
25. Lartillot, N., Philippe, H.: Computing Bayes factors using thermodynamic integration. *Systematic Biology* **55**(2), 195–207 (2006)
26. Li, Y., Mathews, J., Schmidler, S.C.: On Gibbs sampling for endpoint-conditioned neighbor-dependent sequence evolution models. *Journal of Computational and Graphical Statistics* p. 1–6 (Oct 2025)
27. Marcou, Q., Mora, T., Walczak, A.M.: High-throughput immune repertoire analysis with IGOR. *Nat Commun* **9**(1), 561 (2018)
28. Mathews, J., Schmidler, S.: Importance sampling approximation of sequence evolution models with site-dependence. *arXiv preprint arXiv:2507.19659* (2025)
29. Mathews, J., Schmidler, S.: Improved bounds for context-dependent evolutionary models using sequential Monte Carlo. *arXiv preprint arXiv:2511.07736* (2025)
30. Mathews, J., Schmidler, S.C.: Approximating marginal likelihoods in evolutionary models under site-dependence (2024), in preparation
31. Mathews, J., Van Itallie, E., Li, Y., Wiehe, K., Schmidler, S.C.: Computing the inducibility of broadly neutralizing antibodies under a context-dependent model of affinity maturation: applications to sequential vaccine design. *The Journal of Immunology* (Sep 2025)
32. Nielsen, R.: Mapping mutations on phylogenies. *Systematic Biology* **51**(5), 729–739 (2002)
33. Pedersen, A., Wiuf, C., Christiansen, F.: A codon-based model designed to describe lentiviral evolution. *Molecular Biology and Evolution* **15**, 1069–1081 (1998)
34. Ralph, D.K., Matsen, IV, F.A.: Consistency of VDJ rearrangement and substitution parameters enables accurate B cell receptor sequence annotation. *PLOS Computational Biology* **12**(1), 1–25 (2016)
35. Ralph, D.K., Matsen, IV, F.A.: Likelihood-based inference of B cell clonal families. *PLOS Computational Biology* **12**(10), 1–28 (2016)
36. Robinson, D., Jones, D., Kishino, H., Goldman, N., Thorne, J.: Protein evolution with dependence among codons due to tertiary structure. *Molecular Biology and Evolution* **20**, 1692–1704 (2003)
37. Rodrigue, N., Philippe, H., Lartillot, N.: Uniformization for sampling realizations of Markov processes: applications to Bayesian implementations of codon substitution models. *Bioinformatics* **24**(1), 56–62 (2008)
38. Saunders, K.O., Wiehe, K., Tian, M., Acharya, P., Bradley, T., Alam, S.M., Go, E.P., Scearce, R., Sutherland, L., Henderson, R., Hsu, A.L., Borgnia, M.J., Chen, H., Lu, X., Wu, N.R., Watts, B., Jiang, C., Easterhoff, D., Cheng, H.L., McGovern, K., Waddicor, P., Chapdelaine-Williams, A., Eaton, A., Zhang, J., Rountree, W., Verkoczy, L., Tomai, M., Lewis, M.G., Desaire, H.R., Edwards, R.J., Cain, D.W., Bonsignori, M., Montefiori, D., Alt, F.W., Haynes, B.F.: Targeted selection of HIV-specific antibody mutations by engineering B cell maturation. *Science* **366**(6470) (2019)
39. Sethna, Z., Elhanati, Y., Callan, Curtis G, J., Walczak, A.M., Mora, T.: OLGA: fast computation of generation probabilities of B- and T-cell receptor amino acid sequences and motifs. *Bioinformatics* **35**(17), 2974–2981 (Jan 2019)
40. Steel, M.A., Penny, D.: Distributions of tree comparison metrics — some new results. *Systematic Biology* **42**(2), 126–141 (Jun 1993)
41. Steichen, J.M., Lin, Y.C., Havenar-Daughton, C., Pecetta, S., Ozorowski, G., Willis, J.R., Toy, L., Sok, D., Liguori, A., Kratochvil, S., Torres, J.L., Kalyuzhniy, O., Melzi, E., Kulp, D.W., Raemisch, S., Hu, X., Bernard, S.M., Georges, E., Phelps, N., Adachi, Y., Kubitz, M., Landais, E., Umotoy, J., Robinson, A., Briney, B., Wilson, I.A., Burton, D.R., Ward, A.B., Crotty, S., Batista, F.D., Schief, W.R.: A generalized HIV vaccine design strategy for priming of broadly neutralizing antibody responses. *Science* **366**(6470) (2019)
42. Suchard, M.A., Lemey, P., Baele, G., Ayres, D.L., Drummond, A.J., Rambaut, A.: Bayesian phylogenetic and phylodynamic data integration using BEAST 1.10. *Virus Evolution* **4**(1), vey016 (2018)
43. Swanson, O., Martin Beem, J.S., Rhodes, B., Wang, A., Barr, M., Chen, H., Parks, R., Saunders, K.O., Haynes, B.F., Wiehe, K., Azoitei, M.L.: Identification of CDRH3 loops in the B cell receptor repertoire that can be engaged by candidate immunogens. *PLOS Pathogens* **19**(5), 1–21 (2023), publisher: Public Library of Science

44. Tang, T., Van Itallie, E., Wiehe, K., Schmidler, S.C.: Testing for positively-selected mutations in clonal repertoire sequencing using a stochastic model of B cell affinity maturation. (*submitted*) (2023)
45. Teng, G., Papavasiliou, F.N.: Immunoglobulin somatic hypermutation. *Annu Rev Genet* **41**, 107–20 (2007)
46. Tonegawa, S.: Somatic generation of antibody diversity. *Nature* **302**(5909), 575–581 (1983)
47. Walker, L.M., Burton, D.R.: Passive immunotherapy of viral infections: 'super-antibodies' enter the fray. *Nat Rev Immunol* **18**(5), 297–308 (2018)
48. Whidden, C., Claywell, B.C., Fisher, T., Magee, A.F., Fourment, M., Matsen, F.A.: Systematic exploration of the high likelihood set of phylogenetic tree topologies. *Systematic biology* **69**(2), 280–293 (Mar 2020)
49. Wiehe, K., Bradley, T., Meyerhoff, R., Hart, C., Williams, W., Easterhoff, D., Faison, W., Kepler, T., Saunders, K., Alam, S., Bonsignori, M., Haynes, B.: Functional relevance of improbable antibody mutations for HIV broadly neutralizing antibody development. *Cell Host Microbe* **23**(6), 759–765 (2018)
50. Wiehe, K., Saunders, K.O., Stalls, V., Cain, D.W., Venkatayogi, S., Martin Beem, J.S., Berry, M., Evangelous, T., Henderson, R., Hora, B., Xia, S.M., Jiang, C., Newman, A., Bowman, C., Lu, X., Bryan, M.E., Bal, J., Sanzone, A., Chen, H., Eaton, A., Tomai, M.A., Fox, C.B., Tam, Y.K., Barbosa, C., Bonsignori, M., Muramatsu, H., Alam, S.M., Montefiori, D.C., Williams, W.B., Pardi, N., Tian, M., Weissman, D., Alt, F.W., Acharya, P., Haynes, B.F.: Mutation-guided vaccine design: A process for developing boosting immunogens for HIV broadly neutralizing antibody induction. *Cell Host Microbe* **32**(5), 693–709 e7 (2024)
51. Williams, W.T., Clifford, H.T.: On the comparison of two classifications of the same set of elements. *TAXON* **20**(4), 519–522 (1971)
52. Wolpert, R.L., Schmidler, S.C.: α -stable limit laws for harmonic mean estimators of marginal likelihoods. *Statistica Sinica* **22**(3), 1233–1251 (2012)
53. Xie, W., Lewis, P.O., Fan, Y., Kuo, L., Chen, M.H.: Improving marginal likelihood estimation for Bayesian phylogenetic model selection. *Systematic Biology* **60**(2), 150–160 (2010)
54. Yaari, G., Vander Heiden, J.A., Uduman, M., Gadala-Maria, D., Gupta, N., Stern, J.N., O'Connor, K.C., Hafler, D.A., Laserson, U., Vigneault, F., Kleinstein, S.H.: Models of somatic hypermutation targeting and substitution based on synonymous mutations from high-throughput immunoglobulin sequencing data. *Front Immunol* **4**, 358 (2013)

A Pairwise MCMC kernel

Denote the unobserved *full sequence* path as $\mathcal{P} = (\mathcal{P}_1, \dots, \mathcal{P}_n)$, where the path at the i -th site

$$\mathcal{P}_i = (m_i, t_{\text{start}}, t_i^1, \dots, t_i^{m_i}, t_{\text{end}}, b_i^0, b_i^1, \dots, b_i^{m_i})$$

is specified by the number of mutations $m(\mathcal{P}_i) = m_i \in \{0, 1, \dots\}$ occurring at site i along the path, the times $t_i^1, \dots, t_i^{m_i} \in \mathbb{R}_+$ of these mutation events (satisfying $t_{\text{start}} = t_i^0 < t_i^1 < \dots < t_i^{m_i} < t_i^{m_i+1} = t_{\text{end}}$), and the identities $b_i^1, \dots, b_i^{m_i} \in \mathcal{A}$ of the base changes. Note that both $\mathcal{P}_i : [t_{\text{start}}, t_{\text{end}}] \rightarrow \mathcal{A}$ and $\tilde{x}_i : [t_{\text{start}}, t_{\text{end}}] \rightarrow \mathcal{A}^3$ can be viewed as functions, representing the character and the context, respectively, at a specific time stamp. We desire to sample $P_{\mathbf{Q}}(\mathcal{P}_i | \mathcal{P}_{[-i]}, \mathbf{x}, \mathbf{y})$.

For the unobserved full sequence path \mathcal{P} , we can write the the density under the ISM defined by rates \mathbf{Q} as

$$P_{\mathbf{Q}}(\mathbf{y}, \mathcal{P} | \mathbf{x}) = \prod_{i=1}^{\ell} \bar{P}_{\mathbf{Q}}(\mathcal{P}_i)$$

where

$$\bar{P}_{\mathbf{Q}}(\mathcal{P}_i) = \prod_{j=1}^{m_i} \gamma(b_i^j; b_i^{j-1}) \prod_{j=0}^{m_i} e^{-(t_i^{j+1} - t_i^j) \sum_{b \in \mathcal{A}} \gamma(b; b_i^j)}.$$

Similarly, the density for \mathcal{P} under the DSM defined by rate $\tilde{\mathbf{Q}}$ is given by

$$P_{\tilde{\mathbf{Q}}}(\mathbf{y}, \mathcal{P} | \mathbf{x}) = \prod_{j=1}^{\ell} \bar{P}_{\tilde{\mathbf{Q}}}(\mathcal{P}_i | \tilde{x}_i, \tilde{y}_i, \mathcal{P}_{i-1}, \mathcal{P}_{i+1})$$

where

$$\bar{P}_{\tilde{\mathbf{Q}}}(\mathcal{P}_i | \tilde{x}_i, \tilde{y}_i, \mathcal{P}_{i-1}, \mathcal{P}_{i+1}) = \prod_{j=1}^{m_i} \tilde{\gamma}(b_i^j; \tilde{x}_i(t_i^j)) \prod_{j=0}^{m_i} \exp \left\{ - \int_{t_{\text{start}}}^{t_{\text{end}}} \tilde{\gamma}(\cdot; \tilde{x}_i(t)) dt \right\}.$$

Let $\bar{m}'_i := m_{i+1} + m_{i-1}$ be the total number of jumps among the paths \mathcal{P}_{i-1} and \mathcal{P}_{i+1} , and $t_{\text{start}} = t^0 < t^1 < t^2 < \dots < t^{\bar{m}'_i} < t_{\text{end}}$ the corresponding jump times. Denote $\bar{t}_i = \{t^1, \dots, t^{\bar{m}'_i}\}$. The Metropolis-Hastings chain proposes an updated path \mathcal{P}'_i at site i conditional on the neighboring site paths \mathcal{P}_{i-1} and \mathcal{P}_{i+1} using the following algorithm:

Hobolth algorithm:

1. Simulate the bases $\bar{\mathbf{x}}_i = (x_i(t^1), \dots, x_i(t^{\bar{m}'_i}))$ at site i at the neighboring jump times using forward-filtering/backward-sampling.
2. Form the sample path $\mathcal{P}_i = (\mathcal{P}_{i,0} : \dots : \mathcal{P}_{i,\bar{m}'_i})$, where $\mathcal{P}_{i,j}$ is a ‘subpath’ with endpoints $x_i(t^j)$ and $x_i(t^{j+1})$ sampled using single-site endpoint-conditioned sampling techniques [15].

Hobolth algorithm is effectively proposing paths from a position-dependent time-inhomogeneous ISM. In particular, for position i fixing the neighboring path \mathcal{P}_{i-1} and \mathcal{P}_{i+1} , the ISM is defined by rates

$$\mathbf{Q}_{ab}(t | \mathcal{P}_{i-1}, \mathcal{P}_{i+1}) = \tilde{\gamma}(b; (\mathcal{P}_{i-1}(t), a, \mathcal{P}_{i+1}(t))).$$

Note that this CTMC is time-homogeneous within time the interval (t^j, t^{j+1}) for each $i \in \{0, 1, \dots, \bar{m}'_i\}$. Let $\mathbf{Q}^{(i,j)}$ denote the rate matrix for position i within the interval (t^j, t^{j+1}) . Therefore, the density of the characters drawn in step 2, $q(\bar{\mathbf{x}}_i | \tilde{x}_i, \tilde{y}_i, \bar{t}_i, \mathcal{P}_{i-1}, \mathcal{P}_{i+1})$, can be calculated by belief propagation for time-inhomogeneous CTMC. The resulting density of the path drawn in step 3 is given by

$$q(\mathcal{P}_i | \tilde{x}_i, \tilde{y}_i, \bar{t}_i, \mathcal{P}_{i-1}, \mathcal{P}_{i+1}) = \sum_{\bar{\mathbf{x}}_i \in \mathcal{A}^{\bar{m}'_i}} q(\bar{\mathbf{x}}_i | \tilde{x}_i, \tilde{y}_i, \bar{t}_i, \mathcal{P}_{i-1}, \mathcal{P}_{i+1}) \prod_{j=0}^{m_i} P_{\mathbf{Q}^{(i,j)}}(x_i(t^{j+1}), \mathcal{P}_i(t^j : t^{j+1}) | x_i(t^j)),$$

which can be viewed as a mixture model wherein sampling $\bar{\mathbf{x}}_i$ selects the mixture component. Plugging in $P_{\mathbf{Q}^{(i,j)}}$ gives:

$$q(\mathcal{P}_i | \tilde{x}_i, \tilde{y}_i, \bar{t}_i, \mathcal{P}_{i-1}, \mathcal{P}_{i+1}) = P_{\bar{\mathbf{Q}}}(\mathcal{P}_i | \tilde{x}_i, \tilde{y}_i, \mathcal{P}_{i-1}, \mathcal{P}_{i+1}),$$

where the corresponding density of sampling $\bar{\mathbf{x}}_i$ does not appear. Recognizing that we desire to sample

$$p_1(\mathcal{P}_i | \mathbf{x}, \mathbf{y}, \mathcal{P}_{[-i]}) \propto P_{\bar{\mathbf{Q}}}(\mathbf{y}, \mathcal{P} | \mathbf{x}) = \prod_{j=1}^{\ell} \bar{P}_{\bar{\mathbf{Q}}}(\mathcal{P}_i | \tilde{x}_i, \tilde{y}_i, \mathcal{P}_{i-1}, \mathcal{P}_{i+1})$$

where $\mathcal{P}_{[-i]} := (\mathcal{P}_1, \dots, \mathcal{P}_{i-1}, \mathcal{P}_{i+1}, \dots, \mathcal{P}_\ell)$, the acceptance ratio of the Metropolis-Hastings chain is given by

$$a(\mathcal{P}', \mathcal{P}) := \min \left\{ 1, \frac{\bar{P}_{\bar{\mathbf{Q}}}(\mathcal{P}_{i-1} | \tilde{x}_{i-1}, \tilde{y}_{i-1}, \mathcal{P}_i, \mathcal{P}_{i-2}) \bar{P}_{\bar{\mathbf{Q}}}(\mathcal{P}_{i+1} | \tilde{x}_{i+1}, \tilde{y}_{i+1}, \mathcal{P}_i, \mathcal{P}_{i+2})}{\bar{P}_{\bar{\mathbf{Q}}}(\mathcal{P}_{i-1} | \tilde{x}_{i-1}, \tilde{y}_{i-1}, \mathcal{P}_i, \mathcal{P}_{i-2}) \bar{P}_{\bar{\mathbf{Q}}}(\mathcal{P}_{i+1} | \tilde{x}_{i+1}, \tilde{y}_{i+1}, \mathcal{P}_i, \mathcal{P}_{i+2})} \right\}.$$

B Forward-filtering/backward-sampling

Forward-filtering / backward-sampling (FFBS) efficiently draws latent intermediate states or internal states from a time-inhomogeneous CTMC with piecewise constant rates, as used in the Hobolth proposal.

B.1 Sampling the Intermediate States

Recall that we desire to sample $q(\bar{\mathbf{x}}_i | \tilde{x}_i, \tilde{y}_i, \bar{t}_i, \mathcal{P}_{i-1}, \mathcal{P}_{i+1})$ in the first step of Hobolth proposal. Recall that \bar{m}'_i and \bar{t}_i are the total number of jumps and the corresponding jump times among the paths \mathcal{P}_{i-1} and \mathcal{P}_{i+1} , respectively. Denoting $t^0 = t_{\text{start}}$ and $t^{\bar{m}'_i+1} = t_{\text{end}}$, we have

$$\begin{aligned} q(\bar{\mathbf{x}}_i | \tilde{x}_i, \tilde{y}_i, \bar{t}_i, \mathcal{P}_{i-1}, \mathcal{P}_{i+1}) &\propto q\left(x_i(t^1), \dots, x_i(t^{\bar{m}'_i}), x_i(t^{\bar{m}'_i+1}) | x_i(t^0), x_{i-1}, x_{i+1}, y_{i-1}, y_{i+1}, \mathcal{P}_{i-1}, \mathcal{P}_{i+1}\right) \\ &= \prod_{j=0}^{\bar{m}'_i} q\left(x_i(t^{j+1}) | x_i(t^j), x_{i-1}, x_{i+1}, y_{i-1}, y_{i+1}, \mathcal{P}_{i-1}, \mathcal{P}_{i+1}\right) \\ &\stackrel{*}{=} \prod_{j=0}^{\bar{m}'_i} q\left(x_i(t^{j+1}) | x_i(t^j), x_{i-1}, x_{i+1}, y_{i-1}, y_{i+1}, \mathcal{P}_{i-1}, \mathcal{P}_{i+1}\right) \\ &= \prod_{j=0}^{\bar{m}'_i} \left(e^{\mathbf{Q}^{(i,j)}} \right)_{x_i(t^j) x_i(t^{j+1})} \end{aligned}$$

where (*) is invoking the Markov property. We therefore construct Algorithm 1 to sample the intermediate states at a site given its neighboring paths according to the Hobolth proposal.

Algorithm 1: FFBS for sampling intermediate states of site i

Input: Endpoints \tilde{x}_i, \tilde{y}_i ; neighboring paths $\mathcal{P}_{i-1}, \mathcal{P}_{i+1}$; rate matrices $\{\mathbf{Q}^{(i,j)}\}$.
Output: Sequence of intermediate states $\bar{\mathbf{x}}_i = \{x_i(t^1), \dots, x_i(t^{\bar{m}'_i})\}$.

- 1 Initialize transition matrices
- 2 **for** $j \leftarrow 0$ **to** \bar{m}'_i **do** // Initialize transition matrices
- 3 | Calculate $\mathbf{P}^{(i,j)} = e^{\mathbf{Q}^{(i,j)}}$.
- 4 **end**
- 5 **for** $j \leftarrow 1$ **to** \bar{m}'_i **do** // Forward filtering
- 6 | Calculate $v_j(b) = \sum_{a \in \mathcal{A}} v_{j-1}(a) \mathbf{P}_{ab}^{(i,j-1)}$.
- 7 **end**
- 8 **for** $j = \bar{m}'_i$ **to** 1 **do** // Backward sampling
- 9 | Calculate $\Pr(x_i(t^j) = a | x_i(t^0), x_i(t^{j+1}) = b) = \frac{v_j(a) \mathbf{P}_{ab}^{(i,j)}}{\sum_{a'} v_j(a') \mathbf{P}_{a'b}^{(i,j)}}$.
- 10 | Sample $x_i(t^j)$ accordingly.
- 11 **end**

B.2 Sampling the Internal State

We desire to sample $q(s_i | \tilde{x}_i, \tilde{y}_i, \tilde{z}_i, \mathcal{P}_{i-1}^{(\mathbf{x}\mathbf{s}\mathbf{y}\mathbf{z})}, \mathcal{P}_{i+1}^{(\mathbf{x}\mathbf{s}\mathbf{y}\mathbf{z})})$.

$$\begin{aligned}
q(s_i | \tilde{x}_i, \tilde{y}_i, \tilde{z}_i, \mathcal{P}_{i-1}^{(\mathbf{x}\mathbf{s}\mathbf{y}\mathbf{z})}, \mathcal{P}_{i+1}^{(\mathbf{x}\mathbf{s}\mathbf{y}\mathbf{z})}) &\propto q(s_i, y_i, z_i | x_i, x_{i-1}, x_{i+1}, y_{i-1}, y_{i+1}, z_{i-1}, z_{i+1}, \mathcal{P}_{i-1}^{(\mathbf{x}\mathbf{s}\mathbf{y}\mathbf{z})}, \mathcal{P}_{i+1}^{(\mathbf{x}\mathbf{s}\mathbf{y}\mathbf{z})}) \\
&= q(s_i | \tilde{x}_i, \mathcal{P}_{i-1}^{(\mathbf{x}\mathbf{s})}, \mathcal{P}_{i+1}^{(\mathbf{x}\mathbf{s})}) q(y_i, z_i | s_i, \mathcal{P}_{i-1}^{(\mathbf{s}\mathbf{y})}, \mathcal{P}_{i+1}^{(\mathbf{s}\mathbf{y})}, \mathcal{P}_{i-1}^{(\mathbf{s}\mathbf{z})}, \mathcal{P}_{i+1}^{(\mathbf{s}\mathbf{z})}) \\
&= q(s_i | \tilde{x}_i, \mathcal{P}_{i-1}^{(\mathbf{x}\mathbf{s})}, \mathcal{P}_{i+1}^{(\mathbf{x}\mathbf{s})}) q(y_i | \tilde{s}_i, \mathcal{P}_{i-1}^{(\mathbf{s}\mathbf{y})}, \mathcal{P}_{i+1}^{(\mathbf{s}\mathbf{y})}) q(z_i | \tilde{s}_i, \mathcal{P}_{i-1}^{(\mathbf{s}\mathbf{z})}, \mathcal{P}_{i+1}^{(\mathbf{s}\mathbf{z})}),
\end{aligned} \tag{14}$$

where the second equality comes from the conditional independence between \mathbf{y} and \mathbf{z} given \mathbf{s} . Recall that Hobolth algorithm is effectively a time-inhomogeneous CTMC. Using the notations \bar{m}'_i and $\mathbf{Q}^{(i,j)}$ for the pairwise paths $\mathcal{P}_{i-1}^{(\mathbf{x}\mathbf{s})}$ and $\mathcal{P}_{i+1}^{(\mathbf{x}\mathbf{s})}$, we have

$$q(s_i | \tilde{x}_i, \mathcal{P}_{i-1}^{(\mathbf{x}\mathbf{s})}, \mathcal{P}_{i+1}^{(\mathbf{x}\mathbf{s})}) = \left(\prod_{j=0}^{\bar{m}'_i} e^{\mathbf{Q}^{(i,j)}} \right)_{x_i s_i}.$$

Similar calculation can be performed for the latter two terms in (14), giving rise to Algorithm 2 for sampling the internal state of a star-tree.

Algorithm 2: Sampling the internal state s_i

Input: Endpoints $\tilde{x}_i, \tilde{y}_i, \tilde{z}_i$; neighboring paths $\mathcal{P}_{i-1}^{(\mathbf{x}\mathbf{s}\mathbf{y}\mathbf{z})}, \mathcal{P}_{i+1}^{(\mathbf{x}\mathbf{s}\mathbf{y}\mathbf{z})}$; rate matrices $\{\mathbf{Q}^{(i,j)}\}$ for pairwise paths.

Output: Internal state s_i .

- 1 Compute pairwise transition probability $q(s_i | \tilde{x}_i, \mathcal{P}_{i-1}^{(\mathbf{x}\mathbf{s})}, \mathcal{P}_{i+1}^{(\mathbf{x}\mathbf{s})})$.
- 2 Compute pairwise transition probability $q(s_i | \tilde{y}_i, \mathcal{P}_{i-1}^{(\mathbf{s}\mathbf{y})}, \mathcal{P}_{i+1}^{(\mathbf{s}\mathbf{y})})$.
- 3 Compute pairwise transition probability $q(s_i | \tilde{z}_i, \mathcal{P}_{i-1}^{(\mathbf{s}\mathbf{z})}, \mathcal{P}_{i+1}^{(\mathbf{s}\mathbf{z})})$.
- 4 **foreach** $s_i \in \mathcal{A}$ **do** // Calculate unnormalized conditional probability
- 5 $f(s_i) = q(s_i | \tilde{x}_i, \mathcal{P}_{i-1}^{(\mathbf{x}\mathbf{s})}, \mathcal{P}_{i+1}^{(\mathbf{x}\mathbf{s})}) q(s_i | \tilde{y}_i, \mathcal{P}_{i-1}^{(\mathbf{s}\mathbf{y})}, \mathcal{P}_{i+1}^{(\mathbf{s}\mathbf{y})}) q(s_i | \tilde{z}_i, \mathcal{P}_{i-1}^{(\mathbf{s}\mathbf{z})}, \mathcal{P}_{i+1}^{(\mathbf{s}\mathbf{z})})$.
- 6 **end**
- 7 **foreach** $s_i \in \mathcal{A}$ **do** // Normalization
- 8 $\Pr(s_i) = f(s_i) / \sum_{s'_i} f(s'_i)$.
- 9 **end**
- 10 Sample s_i from the categorical distribution $\Pr(s_i)$.

C Star-path MCMC kernel

We introduce a Markov kernel on tree-path space which updates tree-paths component-wise by (randomly or systematically) selecting a tree node \mathbf{s} and proposing a *star-path* change; see Figure S1. Each of the four nodes represents a sequence of length ℓ , e.g. $\mathbf{x} = \{x_1, x_2, \dots, x_{\ell-1}, x_\ell\}$. Let $\mathbf{s}_{-i} = \{s_1, \dots, s_{i-1}, s_{i+1}, \dots, s_\ell\}$, and let $\mathcal{P}^{(\mathbf{x}\mathbf{s})} := (\mathcal{P}_1^{(\mathbf{x}\mathbf{s})}, \dots, \mathcal{P}_\ell^{(\mathbf{x}\mathbf{s})})$ denote an evolutionary path from \mathbf{x} to \mathbf{s} , where $\mathcal{P}_j^{(\mathbf{x}\mathbf{s})}$ is the evolutionary path at site j (from x_j to s_j). We update the *single-site star-path* $\mathcal{P}_i^{(\mathbf{x}\mathbf{s}\mathbf{y}\mathbf{z})} := (\mathcal{P}_i^{(\mathbf{x}\mathbf{s})}, \mathcal{P}_i^{(\mathbf{s}\mathbf{y})}, \mathcal{P}_i^{(\mathbf{s}\mathbf{z})})$ using a Metropolis-Hastings step as follows:

1. Sample character s'_i from the modified Hobolth proposal $q(\cdot)$ (see Appendix) conditioning on $\mathcal{P}_{i-1}^{(\mathbf{x}\mathbf{s}\mathbf{y}\mathbf{z})}$ and $\mathcal{P}_{i+1}^{(\mathbf{x}\mathbf{s}\mathbf{y}\mathbf{z})}$:

$$s'_i \sim q(\cdot | \tilde{x}_i, \tilde{y}_i, \tilde{z}_i, \mathcal{P}_{i-1}^{(\mathbf{x}\mathbf{s}\mathbf{y}\mathbf{z})}, \mathcal{P}_{i+1}^{(\mathbf{x}\mathbf{s}\mathbf{y}\mathbf{z})}).$$

and set $\mathbf{s}' = (s_1, \dots, s_{i-1}, s'_i, s_{i+1}, \dots, s_\ell)$.

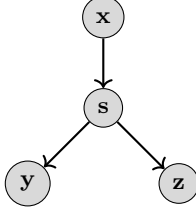


Fig. S1: Example

2. Draw the star-path $\mathcal{P}_i^{(\mathbf{x}\mathbf{s}'\mathbf{y}\mathbf{z})}$ from the Hobolth proposal for pairwise paths (see Appendix A), i.e.

$$\begin{aligned}\mathcal{P}_i^{(\mathbf{x}\mathbf{s}')} &\sim q(\cdot \mid \tilde{x}_i, \tilde{s}'_i, \bar{t}_i^{(\mathbf{x}\mathbf{s})}, \mathcal{P}_{i-1}^{(\mathbf{x}\mathbf{s})}, \mathcal{P}_{i+1}^{(\mathbf{x}\mathbf{s})}) \\ \mathcal{P}_i^{(\mathbf{s}'\mathbf{y})} &\sim q(\cdot \mid \tilde{s}'_i, \tilde{y}_i, \bar{t}_i^{(\mathbf{s}\mathbf{y})}, \mathcal{P}_{i-1}^{(\mathbf{s}\mathbf{y})}, \mathcal{P}_{i+1}^{(\mathbf{s}\mathbf{y})}) \\ \mathcal{P}_i^{(\mathbf{s}'\mathbf{z})} &\sim q(\cdot \mid \tilde{s}'_i, \tilde{z}_i, \bar{t}_i^{(\mathbf{s}\mathbf{z})}, \mathcal{P}_{i-1}^{(\mathbf{s}\mathbf{z})}, \mathcal{P}_{i+1}^{(\mathbf{s}\mathbf{z})})\end{aligned}$$

where $\bar{t}_i^{(\mathbf{x}\mathbf{s})}$ are the times of the jumps among the paths $\mathcal{P}_{i-1}^{(\mathbf{x}\mathbf{s})}$ and $\mathcal{P}_{i+1}^{(\mathbf{x}\mathbf{s})}$, since $\mathcal{P}_i^{(\mathbf{x}\mathbf{s}')} \mathcal{P}_i^{(\mathbf{s}'\mathbf{y})}$ and $\mathcal{P}_i^{(\mathbf{s}'\mathbf{z})}$ are conditionally independent of each other given $\tilde{x}_i, \tilde{y}_i, \tilde{z}_i, \mathcal{P}_{i-1}^{(\mathbf{x}\mathbf{s}\mathbf{y}\mathbf{z})}, \mathcal{P}_{i+1}^{(\mathbf{x}\mathbf{s}\mathbf{y}\mathbf{z})}$ and s'_i under $q(\cdot)$.

3. Accept $\mathcal{P}_i^{(\mathbf{x}\mathbf{s}'\mathbf{y}\mathbf{z})}$ with probability

$$\alpha(\mathcal{P}^{(\mathbf{x}\mathbf{s}'\mathbf{y}\mathbf{z})}, \mathcal{P}^{(\mathbf{x}\mathbf{s}\mathbf{y}\mathbf{z})}) := \min \left\{ 1, a(\mathcal{P}^{(\mathbf{x}\mathbf{s}')} \mathcal{P}^{(\mathbf{x}\mathbf{s})}) a(\mathcal{P}^{(\mathbf{s}'\mathbf{y})} \mathcal{P}^{(\mathbf{s}\mathbf{y})}) a(\mathcal{P}^{(\mathbf{s}'\mathbf{z})} \mathcal{P}^{(\mathbf{s}\mathbf{z})}) \right\},$$

where $a(\cdot, \cdot)$ is the acceptance ratio of the pairwise MCMC kernel given in Appendix A.

Note that q can be viewed as a finite mixture distribution wherein sampling s'_i selects the mixture component:

$$\begin{aligned}q(\mathcal{P}_i^{(\mathbf{x}\mathbf{s}'\mathbf{y}\mathbf{z})} \mid \tilde{x}_i, \tilde{y}_i, \tilde{z}_i, \mathcal{P}_{i-1}^{(\mathbf{x}\mathbf{s}'\mathbf{y}\mathbf{z})}, \mathcal{P}_{i+1}^{(\mathbf{x}\mathbf{s}'\mathbf{y}\mathbf{z})}) \\ = \sum_{s'_i \in \mathcal{A}} q(s'_i \mid \tilde{x}_i, \tilde{y}_i, \tilde{z}_i, \mathcal{P}_{i-1}^{(\mathbf{x}\mathbf{s}\mathbf{y}\mathbf{z})}, \mathcal{P}_{i+1}^{(\mathbf{x}\mathbf{s}\mathbf{y}\mathbf{z})}) q(\mathcal{P}_i^{(\mathbf{x}\mathbf{s}'\mathbf{y}\mathbf{z})} \mid \tilde{x}_i, \tilde{s}'_i, \tilde{y}_i, \tilde{z}_i, \mathcal{P}_{i-1}^{(\mathbf{x}\mathbf{s}\mathbf{y}\mathbf{z})}, \mathcal{P}_{i+1}^{(\mathbf{x}\mathbf{s}\mathbf{y}\mathbf{z})})\end{aligned}$$

where $q(\mathcal{P}_i^{(\mathbf{x}\mathbf{s}'\mathbf{y}\mathbf{z})} \mid \tilde{x}_i, \tilde{s}'_i, \tilde{y}_i, \tilde{z}_i, \mathcal{P}_{i-1}^{(\mathbf{x}\mathbf{s}'\mathbf{y}\mathbf{z})}, \mathcal{P}_{i+1}^{(\mathbf{x}\mathbf{s}'\mathbf{y}\mathbf{z})})$ factors as

$$q(\mathcal{P}_i^{(\mathbf{x}\mathbf{s}')} \mid \tilde{x}_i, \tilde{s}'_i, \bar{t}_i^{(\mathbf{x}\mathbf{s})}, \mathcal{P}_{i-1}^{(\mathbf{x}\mathbf{s})}, \mathcal{P}_{i+1}^{(\mathbf{x}\mathbf{s})}) q(\mathcal{P}_i^{(\mathbf{s}'\mathbf{y})} \mid \tilde{s}'_i, \tilde{y}_i, \bar{t}_i^{(\mathbf{s}\mathbf{y})}, \mathcal{P}_{i-1}^{(\mathbf{s}\mathbf{y})}, \mathcal{P}_{i+1}^{(\mathbf{s}\mathbf{y})}) q(\mathcal{P}_i^{(\mathbf{s}'\mathbf{z})} \mid \tilde{s}'_i, \tilde{z}_i, \bar{t}_i^{(\mathbf{s}\mathbf{z})}, \mathcal{P}_{i-1}^{(\mathbf{s}\mathbf{z})}, \mathcal{P}_{i+1}^{(\mathbf{s}\mathbf{z})}).$$

Hence the density of sampling s'_i does not appear in the Metropolis-Hastings acceptance probability.

D UCA Estimators

As described above, the marginal joint posterior distribution of UCA \mathbf{x} and genealogy g under the ISM is given by

$$p_0(\mathbf{x}, g \mid Y) = p_0(\mathbf{x} \mid Y, g) \pi_0(g \mid Y)$$

which can be sampled by using standard Bayesian phylogenetics packages to draw $g \sim \pi_0(\cdot \mid Y)$ and then applying Felsenstein's pruning to draw $\mathbf{x} \sim p_0(\cdot \mid Y, g)$. The corresponding importance weight of interest

$$\frac{p_1(\mathbf{x}, g \mid Y)}{p_0(\mathbf{x}, g \mid Y)} \propto \frac{p_1(Y \mid \mathbf{x}, g) \zeta_1(\mathbf{x})}{p_0(Y \mid \mathbf{x}, g) \zeta_0(\mathbf{x})} =: w(\mathbf{x}, g) \quad (15)$$

can then be approximated by the following unbiased Monte Carlo estimator:

$$\hat{w}(\mathbf{x}, g) = \frac{1}{m} \sum_{j=1}^m \frac{p_1(Y, Z^{(j)} \mid \mathbf{x}, g)}{p_0(Y, Z^{(j)} \mid \mathbf{x}, g)} \quad (16)$$

Given samples $(\mathbf{x}^{(i)}, Z^{(i)}, g^{(i)})$ for $i = 1, \dots, q$ drawn from the joint posterior $p_0(\mathbf{x}, Z, g \mid Y)$, under the ISM and corresponding importance weights $\hat{w}(\mathbf{x}^{(i)}, g^{(i)})$, (16) weight becomes

$$\hat{w}_j := \frac{\hat{w}(\mathbf{x}^{(j)}, g^{(j)})}{\sum_{i=1}^q \hat{w}(\mathbf{x}^{(i)}, g^{(i)})} \quad \text{where} \quad \hat{w}(\mathbf{x}^{(j)}, g^{(j)}) = \sum_{\{i: x^{(i)}=x^{(j)}\}} \hat{w}(\mathbf{x}^{(i)}, Z^{(i)}, g^{(i)}).$$

We consider two estimators of the UCA which can be obtained directly from \hat{w}_j :

$$\hat{\mathbf{x}}_{\text{MAP}} := \max_x \sum_{i=1}^q \mathbb{1}_{\mathbf{x}=\mathbf{x}^{(i)}} \hat{w}_i \quad \hat{\mathbf{x}}_{\text{MM}} := \left\{ \max_{x_j \in \{\text{A,C,G,T}\}} \sum_{i=1}^q \mathbb{1}_{x_j=x_j^{(i)}} \hat{w}_i \right\},$$

for $\mathbb{1}_{\{\cdot\}}$ an indicator function. $\hat{\mathbf{x}}_{\text{MAP}}$ estimates the *maximum a posteriori* UCA by the sampled UCA with the highest estimated posterior probability, while $\hat{\mathbf{x}}_{\text{MM}}$ estimates the marginal mode nucleotide at each sequence position independently by selecting the most probable nucleotide at each position. For comparison, supposing that \mathbf{x}^* is the true value of the UCA, we also report estimated expected posterior loss under the Hamming distance

$$\hat{E}_{p_1}[d_H(\mathbf{x}, \mathbf{x}^*)] = \frac{1}{q} \sum_{i=1}^q \hat{w}_i d_H(\mathbf{x}^{(i)}, \mathbf{x}^*) \quad \hat{E}_{p_0}[d_H(\mathbf{x}, \mathbf{x}^*)] = \frac{1}{q} \sum_{i=1}^q d_H(\mathbf{x}^{(i)}, \mathbf{x}^*).$$

where $d_H(\mathbf{x}, \mathbf{y}) = \sum_{i=1}^n \delta(x_i \neq y_i)$ is the Hamming distance between sequences \mathbf{x} and \mathbf{y} . The expected loss captures the accuracy of using the entire posterior distribution rather than a single point estimator.

E Variance Decomposition

By law of total variance, we can decompose the variance of the importance weights of tree-paths as

$$\begin{aligned} \text{Var}\left(\frac{p_1(Y, \mathcal{P}^{(g)}, \mathbf{x} \mid g)}{p_0(Y, \mathcal{P}^{(g)}, \mathbf{x} \mid g)}\right) &= \mathbb{E}_{p_0(Z, \mathbf{x} \mid Y, g)} \left(\text{Var}_{p_0(\mathcal{P}^{(g)} \mid Y, Z, \mathbf{x}, g)} \left(\frac{p_1(Y, Z, \mathcal{P}^{(g)}, \mathbf{x} \mid g)}{p_0(Y, Z, \mathcal{P}^{(g)}, \mathbf{x} \mid g)} \mid Z, \mathbf{x} \right) \right) \\ &\quad + \text{Var}_{p_0(Z, \mathbf{x} \mid Y, g)} \left(\mathbb{E}_{p_0(\mathcal{P}^{(g)} \mid Y, Z, \mathbf{x}, g)} \left(\frac{p_1(Y, Z, \mathcal{P}^{(g)}, \mathbf{x} \mid g)}{p_0(Y, Z, \mathcal{P}^{(g)}, \mathbf{x} \mid g)} \mid Z, \mathbf{x} \right) \right) \\ &= \mathbb{E} \left(\text{Var} \left(\frac{p_1(Y, Z, \mathcal{P}^{(g)}, \mathbf{x} \mid g)}{p_0(Y, Z, \mathcal{P}^{(g)}, \mathbf{x} \mid g)} \mid Z, \mathbf{x} \right) \right) + \text{Var}_{p_0(Z, \mathbf{x} \mid Y, g)} \left(\frac{p_1(Y, Z, \mathbf{x} \mid g)}{p_0(Y, Z, \mathbf{x} \mid g)} \right). \end{aligned} \quad (17)$$

The first component is the expected conditional variance due to the stochasticity in the path samples given the internal sequence \mathbf{x} and Z . The second component is the variance of the conditional expectation, the variance across the different possible internal sequence configurations. One option to control the variance is to condition more tightly on the internal sequences, which motivates the stratified sampling.

Our stratified sampling algorithm reduces variance by uniformly (over \mathbf{x} and Z) bounding the first variance term in (7), which is conceptually similar to Rao-Blackwellization. However, the stratified sampling does not control the second term in (17), which relates to the distance between the marginal joint distributions of $\mathbf{x}, Z \mid g, Y$ under the ISM vs DSM distributions.

At first glance, Table 2 appears to suggest that the stratified sampling strategy yields higher variance than standard importance sampling, which would seem to contradict the above analysis. However, this is not the case, as the reported ESS for stratified sampling corresponds to roughly 1.11 effective samples of *internal sequences* (\mathbf{x}, Z) . Since the first term in (17) can be made arbitrarily small using the edge-weight estimator in [30], the remaining variance primarily arises from the distance between the instrumental (ISM) and target (DSM) distributions. This observation motivates the sequential Monte Carlo strategy that progressively bridges these two distributions.

F Experiments

Model Parameters For the DSM, we consistently use the mutation rates specified by the ARMADiLLO model [49]. For the ISM, we employ the corresponding mean-field approximation. This choice helps reduce the possibility that differences in the inferred trees or UCAs between the ISM and DSM arise from disparities in the underlying rate parameters rather than from the presence or absence of context-dependent effects.

Simulation Details For Table 3(a), we performed two simulations for CDR3 sequences and eight simulations for full-length BCR sequences. For Table 3(b), we conducted ten simulations for full-length BCR sequences. Evaluating the weight of a single tree on CDR3 sequences using the SMC algorithm with 1024 particles and 32 intermediate distributions requires approximately 12 hours on 45 CPU cores. Holding all other configurations fixed—including the tree topology and branch lengths—the CPU time increases approximately linearly with sequence length. For longer sequences, however, achieving stable estimates may require additional intermediate distributions and a larger number of particles, which can further increase the overall running time.

CH235 The amino acid frequencies in the CDR3 region of the 55 clonal members used in the experiments are shown in Figure S2. The reconstructed CH235 clone under both the ISM and DSM frameworks are presented in Figure S3.

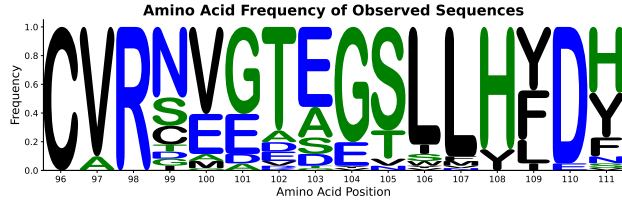
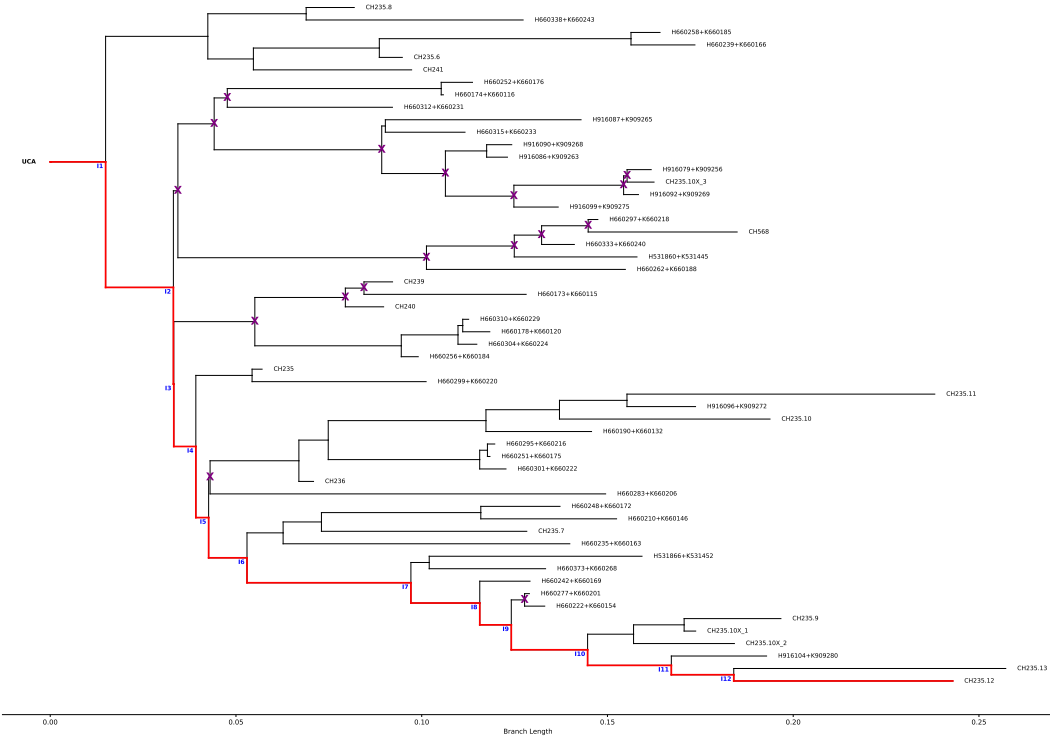
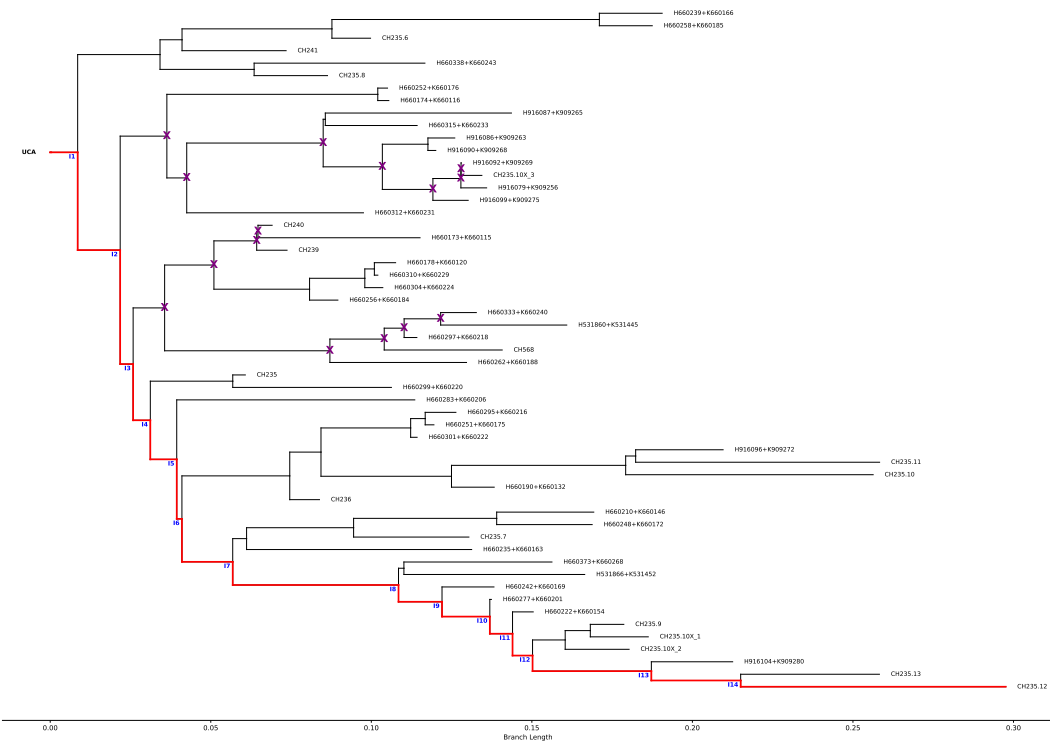


Fig. S2: Frequency of observed sequences in CH235 clone.



(a) MAP CH235 clone under the ISM+NGS.



(b) MAP CH235 clone under the DSM+NGS.

Fig. S3: The CH235 lineage includes several antibodies, notably CH235, CH235.9, and CH235.12, each representing different stages of somatic hypermutation and maturation. Among these, CH235.12 is recognized as the most mature and broad member, capable of neutralizing approximately 90% of circulating HIV-1 strains with high potency. This antibody has been extensively studied for its potential as a template for vaccine design. The red paths highlight the trajectory leading to CH235.12, and nodes marked with an 'X' indicate subclones where the two trees differ in their inferred structures.